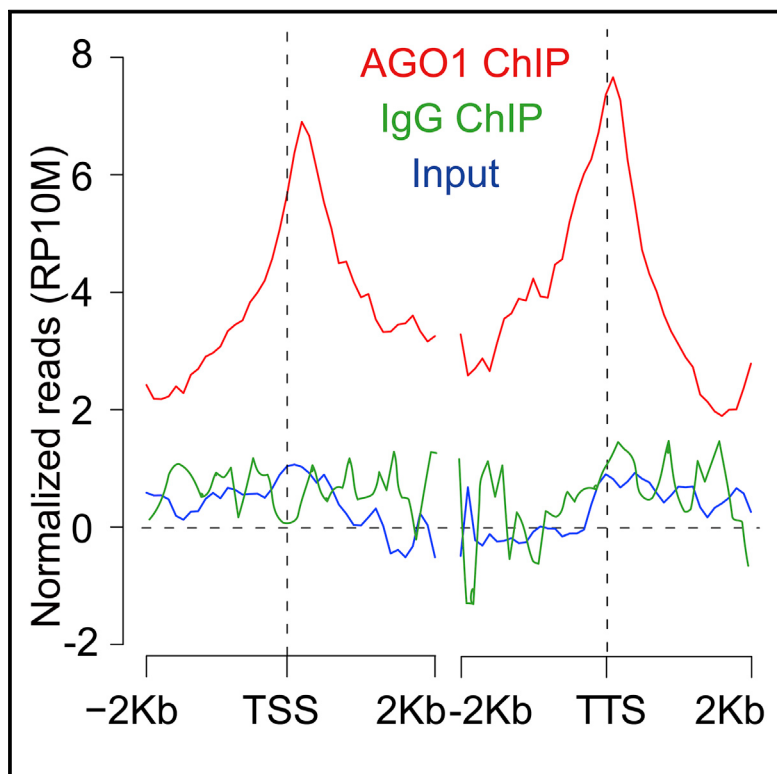


Developmental Cell

Arabidopsis ARGONAUTE 1 Binds Chromatin to Promote Gene Transcription in Response to Hormones and Stresses

Graphical Abstract



Authors

Chang Liu, Ying Xin, Le Xu, ...,
Daoxin Xie, Yule Liu, Yijun Qi

Correspondence

qiyijun@tsinghua.edu.cn

In Brief

Argonaute (AGO) proteins are well known to bind small RNAs and direct post-transcriptional gene silencing. Liu et al. uncover an unsuspected role for *Arabidopsis* AGO1 in direct chromatin binding to promote gene transcription in responses to stimuli, including hormones and stresses. AGO1 binding requires small RNAs and the SWI/SNF chromatin-remodeling complexes.

Highlights

- AGO1 binds to the chromatin of transcribed genes
- AGO1 binding to chromatin requires small RNAs and SWI/SNF
- AGO1 promotes the transcription of AGO1-bound genes
- Hormone and stress stimuli trigger AGO1 binding to stimulus-responsive genes



Arabidopsis ARGONAUTE 1 Binds Chromatin to Promote Gene Transcription in Response to Hormones and Stresses

Chang Liu,^{1,3,4,7} Ying Xin,^{1,3,4,7} Le Xu,^{1,7} Zhaokui Cai,⁵ Yuanchao Xue,⁵ Yong Liu,⁶ Daoxin Xie,^{1,2} Yule Liu,^{1,2} and Yijun Qi^{1,2,8,*}

¹Center for Plant Biology, School of Life Sciences, Tsinghua University, Beijing 100084, China

²Tsinghua-Peking Center for Life Sciences, Beijing 100084, China

³College of Biological Sciences, China Agricultural University, Beijing 100193, China

⁴National Institute of Biological Sciences, Beijing 102206, China

⁵Key Laboratory of RNA Biology, Institute of Biophysics, Chinese Academy of Sciences, Beijing 100101, China

⁶Plant Protection Institute, Hunan Academy of Agricultural Sciences, Changsha 410125, China

⁷These authors contributed equally

⁸Lead Contact

*Correspondence: qiyijun@tsinghua.edu.cn

<https://doi.org/10.1016/j.devcel.2017.12.002>

SUMMARY

Conventional RNA interference (RNAi) pathways suppress eukaryotic gene expression at the transcriptional or post-transcriptional level. At the core of RNAi are small RNAs (sRNAs) and effector Argonaute (AGO) proteins. *Arabidopsis* AGO1 is known to bind microRNAs (miRNAs) and post-transcriptionally repress target genes in the cytoplasm. Here, we report that AGO1 also binds to the chromatin of active genes and promotes their transcription. We show that sRNAs and SWI/SNF complexes associate with nuclear AGO1 and are required for AGO1 binding to chromatin. Moreover, we show that various stimuli, including plant hormones and stresses, specifically trigger AGO1 binding to stimulus-responsive genes. Finally, we show that AGO1 facilitates the induction of genes in jasmonate (JA) signaling pathways and the activation of JA responses. Our findings suggest that, by binding and facilitating the expression of stimuli-specific genes, AGO1 may regulate diverse signaling pathways and associated biological processes.

INTRODUCTION

The Argonaute (AGO) family proteins are known as core effectors of RNA interference (RNAi) pathways in eukaryotes. AGO proteins associate with different classes of small RNAs (sRNAs) that are processed from double-stranded or stem-loop structured precursor RNAs by Dicer or Dicer-like (DCL) proteins (Baulcombe, 2004; Kim, 2005). Guided by sRNAs, AGO proteins bind target sequences through base pairing, which causes the cleavage of target RNAs and/or the recruitment of cofactors to

mediate post-transcriptional gene silencing (PTGS) or transcriptional gene silencing (TGS) (Fang and Qi, 2016; Joshua-Tor and Hannon, 2011; Meister, 2013).

The roles of AGO proteins in TGS by guiding epigenetic modifications of chromatin were first illustrated in plants and fungi. In *Arabidopsis thaliana*, AGO4 binds 24-nt small interfering RNAs (siRNAs) and recruits DNA methyltransferase DRM2 to direct *de novo* DNA methylation at target loci, through base pairing between the siRNAs and cognate nascent transcripts produced by RNA polymerase V (Pol V) and interaction between AGO4 and Pol V (Law and Jacobsen, 2010; Matzke and Mosher, 2014; Wendte and Pikaard, 2017; Zhang and Zhu, 2011). Likewise, in *Schizosaccharomyces pombe*, Ago1 loaded with siRNAs is localized to pericentromeric regions and facilitates H3K9 methylation by recruiting H3K9 methyltransferase Clr4 (Martienssen and Moazed, 2015; Volpe and Martienssen, 2011). Later, a parallel mechanism involving the PIWI subfamily proteins and PIWI-interacting RNA (piRNA) was found to operate in the germlines of metazoans to repress transcription of transposons and their mobilization (Aravin et al., 2007; Iwasaki et al., 2015).

Emerging evidence supports that AGO proteins can also contribute to transcriptional regulation through mechanisms different from conventional RNAi. For instance, *Drosophila* AGO2 plays a role in repressing gene transcription (Taliaferro et al., 2013). AGO2 and Dicer 2 (DCR2) interact with both euchromatin and RNA polymerase II (Pol II) and inhibit the expression of heat-shock genes in non-heat-shocked cells by controlling the processivity of Pol II (Cernilgar et al., 2011). AGO2 has also been implicated in insulator function through interaction with CTCF and CP190 in an RNAi-independent manner (Moshkovich et al., 2011). In human cancer cells, Ago1 associates with Pol II and the promoters of transcriptionally active genes and affects active transcription (Huang et al., 2013). Interestingly, in *Caenorhabditis elegans*, AGO family proteins CSR-1 and ALG-3/4, which bind 26G- and 22G-RNA, respectively, positively regulate the transcription of spermiogenic target genes, and provide a



paternal memory of germline gene expression (Conine et al., 2013; Seth et al., 2013). The mechanism of such transcriptional gene activation remains to be elucidated.

Arabidopsis AGO1 is the founding member of the AGO family (Bohmert et al., 1998). AGO1 predominantly binds microRNAs (miRNAs) and post-transcriptionally represses target genes via mRNA cleavage and/or translational repression in the cytoplasm (Baulcombe, 2004; Fang and Qi, 2016; Rogers and Chen, 2013; Voinnet, 2009). We and others have previously shown that AGO1 is also localized in the nucleus (Dolata et al., 2016; Fang and Spector, 2007; Wang et al., 2011b). Interestingly, AGO1 has recently been implicated in transcriptional regulation of a small subset of miRNAs in plants under salt stress conditions (Dolata et al., 2016).

In this study, we investigate the role of nuclear AGO1 in gene regulation on a genome-wide scale. We show that AGO1 binds to the chromatin of genic regions and positively regulates target gene transcription. We demonstrate that AGO1 binding to chromatin requires sRNAs and the SWI/SNF chromatin-remodeling complexes. Unexpectedly, and perhaps more importantly, we find that AGO1 binding to its target genes is responsive to plant hormones, biotic stresses, and abiotic stresses. Our findings thus reveal an unsuspected role for AGO1 in promoting gene transcription in response to plant hormones and stresses.

RESULTS

Nuclear AGO1 Preferentially Binds to Genic Regions in *Arabidopsis*

We first confirmed the localization of AGO1 in the nucleus by transiently expressing N-terminally GFP-tagged AGO1 (GFP-AGO1) in *Arabidopsis* protoplasts (Figure 1A). We then examined whether nuclear AGO1 could bind to chromatin by subcellular fractionation experiments. Indeed, AGO1 was detected in the chromatin-associated cell fraction (Figure 1B).

The association of AGO1 with chromatin prompted us to identify the AGO1 binding sites within the genome. We prepared nuclear extracts from the wild-type (Col-0) plants and performed chromatin immunoprecipitation (ChIP) combined with high-throughput sequencing (ChIP-seq) using an AGO1-specific antibody (Qi et al., 2005) and immunoglobulin G (IgG) as a control (Table S1). We employed the MACS (model-based analysis for ChIP-seq) peaking calling method (Zhang et al., 2008) to identify AGO1-enriched regions. We obtained 940 AGO1 peaks that were reproducible in two biological replicates (Table S2). None of the AGO1 peaks can be identified in IgG ChIP-seq. Statistical analysis revealed that AGO1 peaks were significantly over-represented within genic regions (Figure 1C). Genic regions were broken down into 5' UTR, 3' UTR, exon, intron, promoter, and 3'-flanking 1-kb region. AGO1 was present throughout the genic regions with two peaks near the transcription start sites (TSSs) and the transcription termination sites (TTSSs), respectively (Figures 1D, 1E, and S1), which resembles the pattern of Pol II distribution on transcribed genes (Adelman and Lis, 2012; Hajheidari et al., 2013) (also see Figure 3C in this study). The binding of AGO1 to a panel of randomly selected sites was confirmed by ChIP-qPCR with Col-0 and ago1-36 mutant plants (Figure 1F).

Chromatin-Bound AGO1 Positively Regulates Gene Expression

The binding of AGO1 to the chromatin of genes raised the question whether AGO1 could regulate gene expression. To address this, we performed mRNA sequencing (RNA-seq) experiments with Col-0 as well as ago1-36 (Table S1). Analysis of RNA-seq data revealed that in Col-0, AGO1-bound genes generally showed higher expression compared to non-AGO1-bound genes (Figure 2A), suggesting that AGO1 binding is positively correlated with the level of gene expression.

Further analyses showed that the expression levels of miRNA-targeted genes in ago1-36 were higher than those in Col-0, as expected (Figure 2B, left). The levels of randomly selected non-AGO1-bound control genes were comparable in Col-0 and ago1-36 (Figure 2B, right). However, the levels of AGO1-bound genes were generally reduced in ago1-36 (Figure 2B, middle). Among AGO1-bound genes, 193 genes were significantly downregulated while 22 were upregulated in ago1-36 (Figures 2C and S1 and Table S2). To validate the mRNA-seq results, we measured the expression levels of the selected genes by RT-qPCR. While one miRNA-targeted gene showed elevated expression, all downregulated AGO1-bound genes examined were confirmed to have reduced expression in ago1-36 (Figure 2D). These genes also have reduced expression in the hypomorphic mutant ago1-25 (Morel et al., 2002) (Figure 2D). Collectively, these results suggest that, different from cytoplasmic AGO1, chromatin-bound AGO1 positively regulates gene expression.

As AGO1 binds to the chromatin of its target genes, the regulation of the target genes by AGO1 likely occurs at the transcriptional level. To test this, we first detected the transcript levels of the selected AGO1-bound or non-AGO1-bound genes by RT-qPCR with exon- or intron-specific primers. If AGO1 transcriptionally promotes gene expression, the levels of both exonic and intronic amplicons were expected to decline in ago1-36 and ago1-25, as a result of declined nascent pre-mRNA levels. Indeed, we observed a dramatic decrease in the levels of both exonic and intronic amplicons in ago1-36 and ago1-25 (Figure 2E), supporting the notion that AGO1 promotes gene transcription.

Positive Regulation of Gene Transcription by AGO1 Occurs Genome-wide

To evaluate the effect of AGO1 on gene transcription on a genome-wide scale, we employed the global run-on sequencing (GRO-seq) assay, which captures nascent transcripts independent of RNA stability (Core et al., 2008; Hetzel et al., 2016) (Table S1). We found that the levels of nascent transcripts of AGO1-bound genes, but not those of non-AGO1-bound genes, were significantly reduced in ago1-36 (Figures 3A and S1 and Table S2). Among AGO1-bound genes, 635 genes had significantly reduced transcription rates in ago1-36 (Table S2). To validate our GRO-seq results, we performed nuclear run-on assays, which quantitatively measure gene transcription rates. Consistently, we found that the ago1-36 mutation caused a marked decrease in the transcription rates of all examined AGO1 target genes (Figure 3B).

GRO-seq maps the position and amount of transcriptionally engaged Pol II (Core et al., 2008; Hetzel et al., 2016). Our

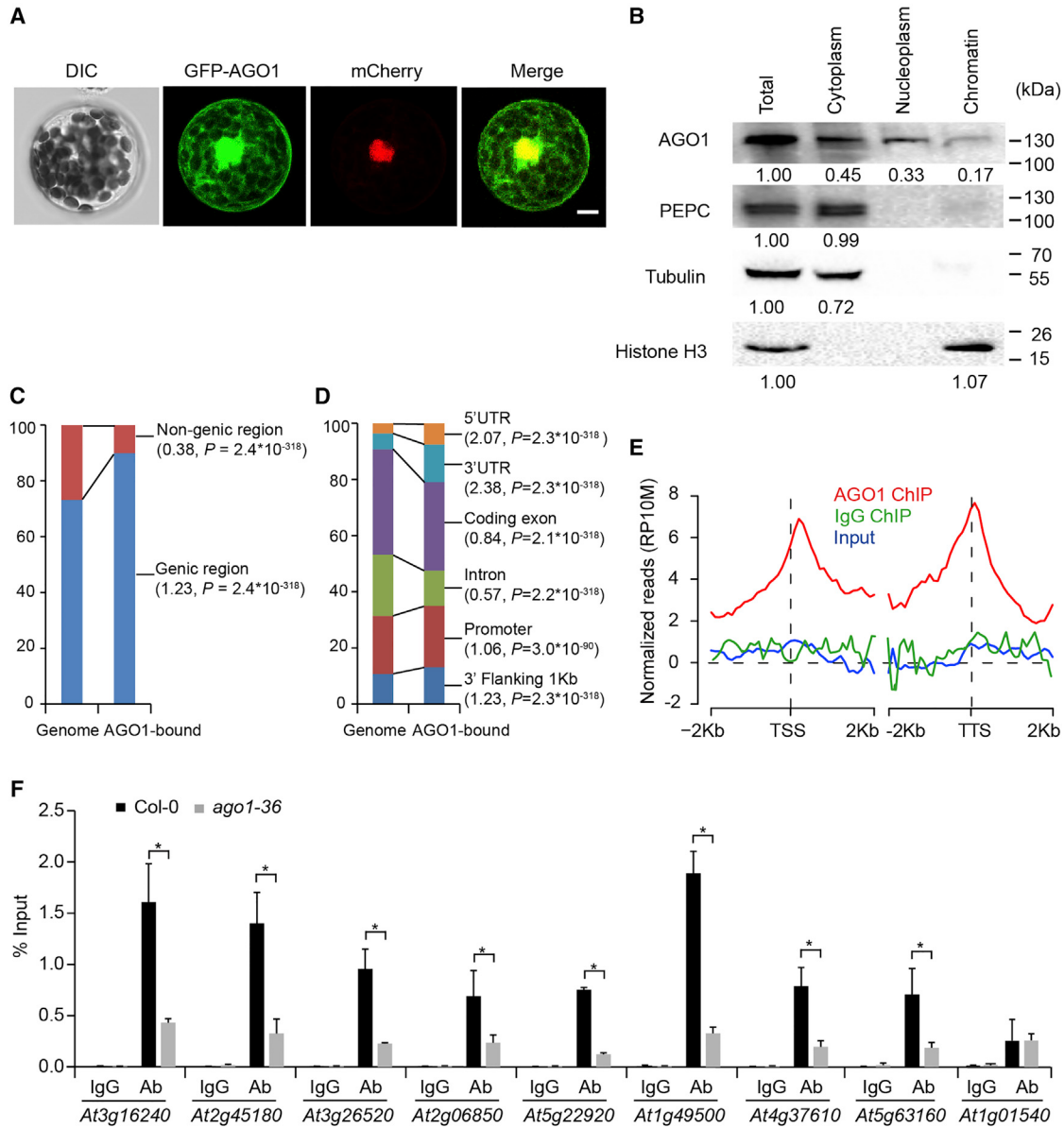


Figure 1. Nuclear AGO1 Preferentially Binds to the Chromatin of Genes in *Arabidopsis*

(A) Localization of GFP-AGO1 in *Arabidopsis* protoplasts. SV40NLS-mCherry was used to label the nucleus. Bar, 10 μ M. DIC, differential interference contrast.

(B) Detection of AGO1 in total protein extract as well as cytoplasmic, nucleoplasmic, and chromatin-associated fractions by western blot. Phosphoenolpyruvate carboxylase (PEPC) and tubulin were detected and used as cytoplasmic markers, and histone H3 was used as a marker for the chromatin-associated fraction. Note that five times more extracts were loaded for the nucleoplasmic and chromatin-associated fractions. The intensities of the bands were quantified and presented. The positions of molecular weight markers are shown on the right.

(C) Percentages of genic and non-genic regions that are associated with AGO1 peaks identified by ChIP-seq. The abundances of genic and non-genic regions in the *Arabidopsis* genome are shown for comparison. The numbers in the parentheses indicate the enrichment ratio relative to the genome. The p values were calculated from Fisher's exact test.

(D) Percentages of promoter, 5' UTR, exon, intron, 3' UTR, and 3' flanking 1-kb region that are associated with AGO1 peaks identified by ChIP-seq. The abundances of those regions in the *Arabidopsis* genome are shown for comparison. The numbers in the parentheses present the enrichment ratio relative to the genome. The p values were calculated from Fisher's exact test.

(E) A metaplot showing the distribution of AGO1 ChIP-seq reads as normalized read counts per 10 million (RP10M) within each 100-bp interval around TSS and TTS of AGO1-bound genes. The distributions of reads from IgG ChIP-seq and input DNA samples are shown as background controls.

(F) Validation of randomly selected AGO1-bound genes by ChIP-qPCR. ChIP was performed in 10-day-old wild-type (Col-0) and *ago1-36* using AGO1-specific antibody (Ab) or IgG. *At1g01540*, a non-AGO1-bound gene, served as a negative control. Error bars indicate standard deviations of three biological replicates. Asterisks indicate significant differences between the indicated samples ($p < 0.05$, t test).

See also Figure S1 and Tables S1 and S2.

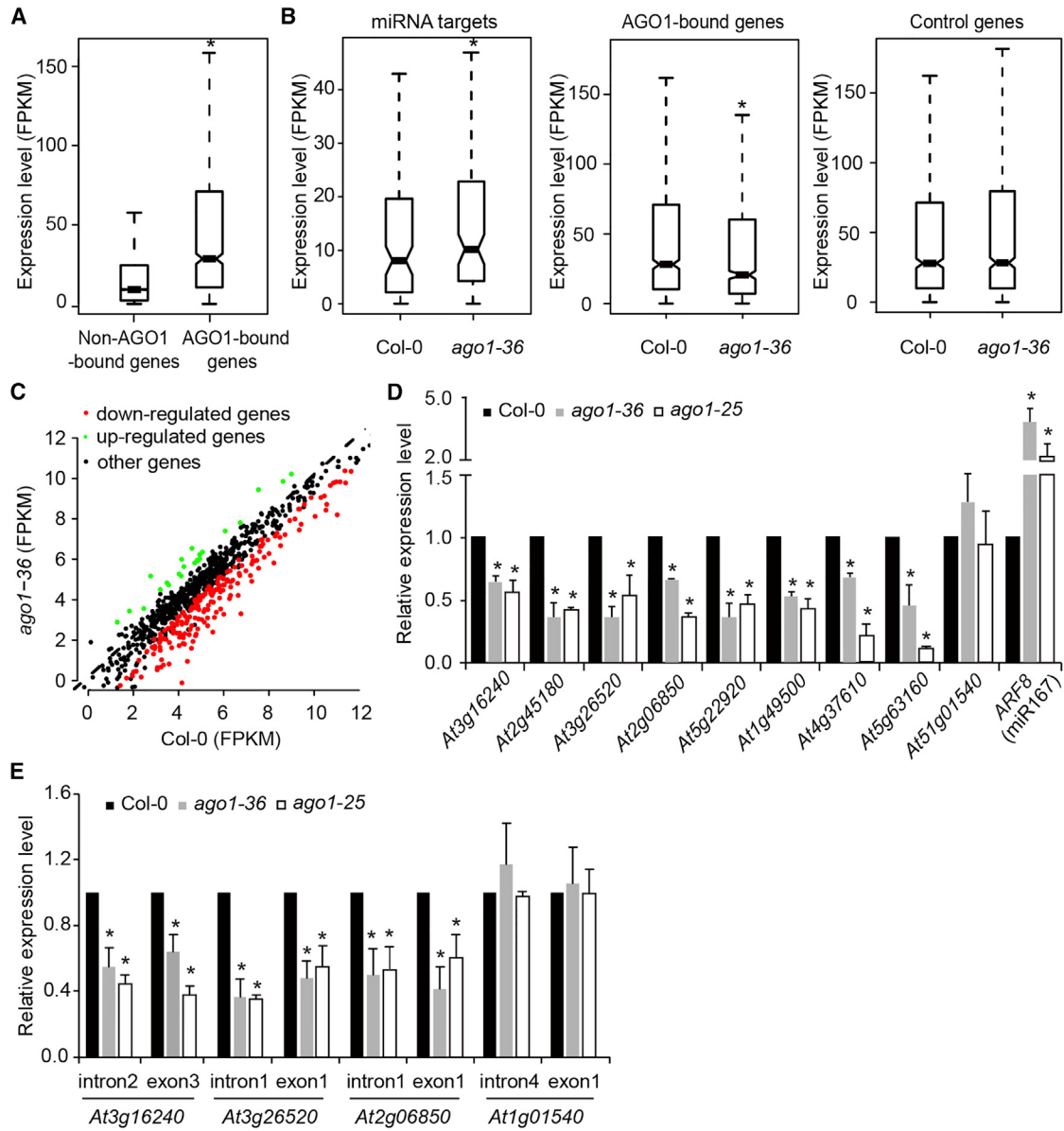


Figure 2. Chromatin-Bound AGO1 Positively Regulates Gene Expression

(A) Box plots illustrating the expression levels of AGO1-bound and non-AGO1-bound genes in 10-day-old Col-0. The asterisk indicates a significant difference (two-sided Wilcoxon test, $p < 0.01$). FPKM, fragments per kilobase million.

(B) Box plots illustrating the expression levels of miRNA targets and AGO1-bound genes and control genes in 10-day-old Col-0 and ago1-36. Control genes are randomly selected non-AGO1-bound genes with similar levels of expression as AGO1-bound genes. Asterisks indicate significant differences between Col-0 and ago1-36 (two-sided Wilcoxon test, $p < 0.01$).

(C) Scatterplots of FPKM values of all AGO1-bound genes in 10-day-old Col-0 and ago1-36 seedlings.

(D) Detection of the expression levels of AGO1-bound genes and miRNA targets in 10-day-old Col-0, ago1-36, and ago1-25 seedlings by RT-qPCR. At1g01540, a non-AGO1-bound gene, served as a negative control. Error bars indicate SDs of three biological replicates. Asterisks indicate significant differences between Col-0, ago1-36, and ago1-25 ($p < 0.05$, t test).

(E) Detection of the exonic and intronic amplicons of AGO1-bound genes in 10-day-old Col-0, ago1-36, and ago1-25 seedlings by RT-qPCR. At1g01540, a non-AGO1-bound gene, served as a negative control. Error bars indicate SDs of three biological replicates. Asterisks indicate significant differences between Col-0, ago1-36, and ago1-25 ($p < 0.05$, t test).

See also Figure S1 and Tables S1 and S2.

GRO-seq data suggested that, at AGO1 target genes, the densities of engaged Pol II were decreased throughout the genic regions in ago1-36 (Figures 3A and S1). After confirming that

the overall abundances of either non-phosphorylated or phosphorylated forms of Pol II were not decreased in ago1-36 (Figure S2A), we examined Pol II density at AGO1 target genes by

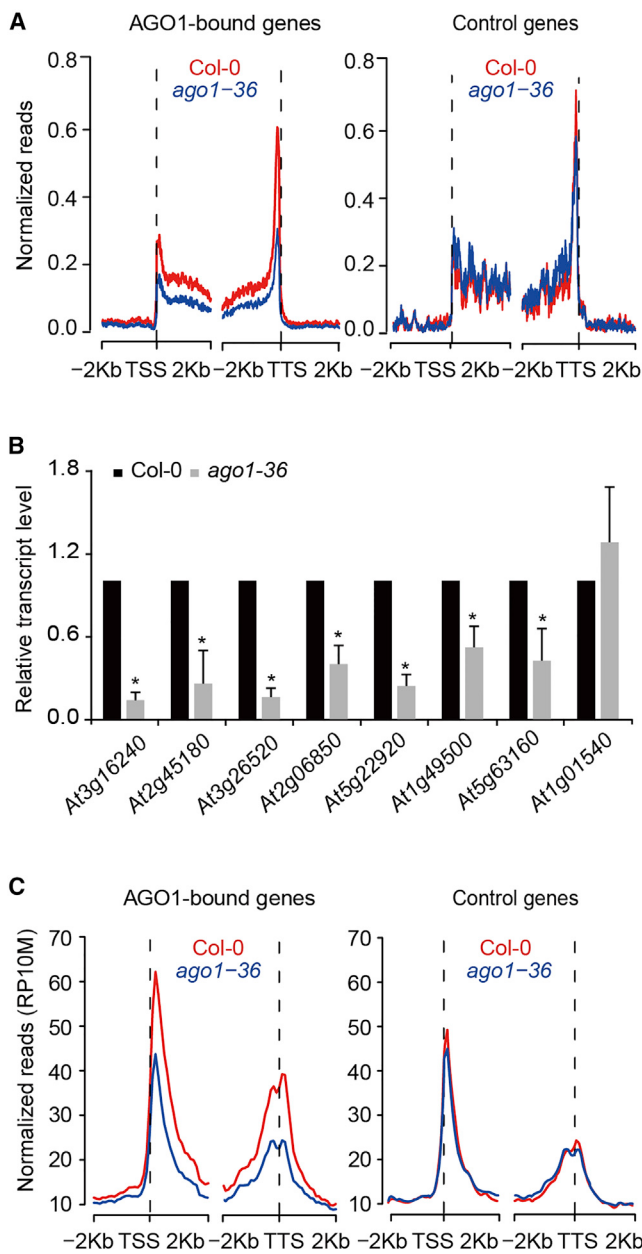


Figure 3. Positive Regulation of Gene Expression by AGO1 Occurs at the Transcriptional Level

(A) Metaplots showing the distribution of GRO-seq reads as normalized read counts within each 100-bp interval around TSS and TTS of AGO1-bound genes and control genes in Col-0 and *ago1-36*. Control genes are randomly selected non-AGO1-bound genes with similar levels of expression as AGO1-bound genes.

(B) Detection of the transcription levels of AGO1-bound genes in 10-day-old Col-0 and *ago1-36* seedlings by nuclear run-on assay. Error bars indicate SDs of three biological replicates. Asterisks indicate significant differences between Col-0 and *ago1-36* ($p < 0.05$, t test).

(C) Metaplots showing the distribution of Pol II ChIP-seq reads as RP10M within each 100-bp interval around TSS and TTS of AGO1-bound genes and control genes in Col-0 and *ago1-36*. Control genes are randomly selected non-AGO1-bound genes with similar levels of expression as AGO1-bound genes. See also Figures S1 and S2 and Tables S1 and S2.

ChIP-seq using an antibody that recognizes both non-phosphorylated and phosphorylated forms of Pol II (total Pol II) (Table S1). We found that total Pol II was enriched on AGO1 target loci with two peaks near TSS and TTS (Figures 3C and S1), which were indicative of promoter-proximal and 3' pausing of Pol II, respectively (Adelman and Lis, 2012; Hajheidari et al., 2013). In agreement with the GRO-seq results, the enrichment of total Pol II at AGO1 target genes was found to be much lower in *ago1-36* (Figures 3C and S1). To validate the ChIP-seq results, we performed Pol II ChIP-qPCR and found that all examined AGO1 targets had markedly reduced Pol II occupancy in *ago1-36* (Figures S2B–S2D). Taken together, our results suggest that AGO1 promotes gene expression through assisting Pol II recruitment.

In yeast and humans, non-phosphorylated Pol II, phosphorylated Pol II at Ser5 (Ser5P), and phosphorylated Pol II at Ser2 (Ser2P) represent the pre-initiation, initiation, and elongation forms of Pol II respectively (Hajheidari et al., 2013; Heidemann et al., 2013). Pol II phosphorylation at Ser5 and Ser2 also occurs in *Arabidopsis* and may mark different steps of transcription (Hajheidari et al., 2013). To investigate the effect of AGO1 on the enrichment of different forms of Pol II, we performed ChIP-seq in Col-0 and *ago1-36* using antibodies against Pol II Ser5P and Ser2P, respectively (Table S1). We found that the enrichment of Pol II Ser5P peaked around the TSS as well as the TTS in *Arabidopsis*, while Pol II Ser2P reached the top level near the TTS (Figures S2E and S2G). The *ago1-36* mutation caused decreased accumulation of Pol II Ser5P and Ser2P throughout the genic regions of AGO1 target genes (Figures S2E and S2G). These results were further confirmed by greatly reduced occupancy of Pol II Ser5P and Ser2P at selected gene loci, as determined by ChIP-qPCR (Figures S2F and S2H). Our results thus suggest that AGO1 dysfunction affects the enrichment of phosphorylated Pol II at AGO1 target genes during each step of transcription.

Small RNAs Are Involved in AGO1 Binding to the Chromatin

AGO proteins are usually guided to their targets by sRNAs through sequence complementarity. We asked whether AGO1 binding to chromatin involves sRNAs. We first examined whether nuclear AGO1 associates with sRNAs originated from AGO1-bound regions. We immunoprecipitated AGO1 from the nuclear extracts from Col-0 (Figure S3A), and analyzed nuclear AGO1-associated sRNAs by sRNA sequencing (sRNA-seq) (Table S1). Analyses of the sRNA-seq data revealed that nuclear AGO1 mainly associated with sRNAs that have a 5'-terminal uridine (U) and are 21 nt in length (Figures S3B and S3C), which are consistent with the intrinsic properties of AGO1 (Mi et al., 2008; Montgomery et al., 2008). Nuclear AGO1-bound sRNAs were found to have a lower proportion of miRNAs, compared with total AGO1-bound sRNAs (Mi et al., 2008), whereas trans-acting small interfering RNAs (tasiRNAs) (Fang and Qi, 2016), for unknown reasons, were over-represented in nuclear AGO1-bound sRNAs. The proportions of other classes of sRNAs did not substantially change (Figure S3D). Nuclear AGO1-associated sRNAs were significantly enriched at AGO1-bound genes (Figure 4A). Specifically, sRNAs were detectable at 55% of AGO1-bound genes (Table S2), as exemplified by the target loci shown in Figures 4B and S1.

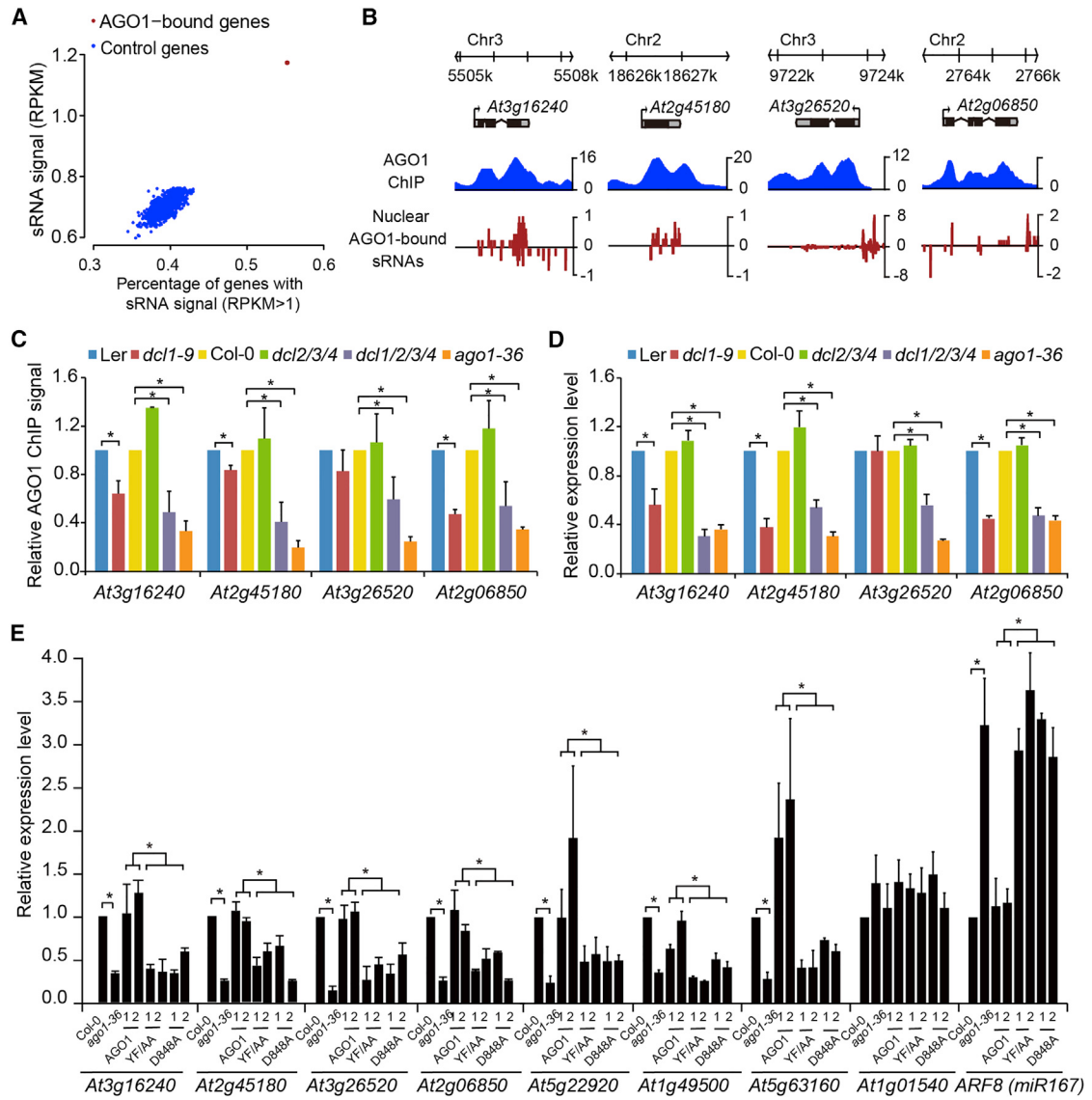


Figure 4. sRNAs Are Involved in AGO1 Binding to the Chromatin

(A) Scatterplots showing the percentages of AGO1-bound genes (red) and control genes (blue) with sRNA signals and the abundances of sRNAs at these groups of genes. Control genes are randomly selected 1,000 groups of non-AGO1-bound genes with similar levels of expression as AGO1-bound genes. The percentages of genes with sRNA reads per kilobase per million mapped reads (RPKM) > 1 are plotted on the x axis. The median values of sRNA signals for shuffled gene sets are plotted on the y axis.

(B) Genome browser views of sRNA and AGO1 ChIP signals at AGO1-bound genes in Col-0, with normalized read counts per million along the y axis. More examples are available in Figure S1.

(C) Detection of AGO1 occupancy at the AGO1 target genes in the 10-day-old indicated plants by ChIP-qPCR. AGO1 ChIP signals in the mutants are presented in relation to those in Col-0 or Ler (arbitrarily set to 1.0). Error bars indicate SDs of three biological replicates. Asterisks indicate significant differences between the indicated samples ($p < 0.05$, t test).

(D) Detection of the expression levels of AGO1 target genes in the indicated 10-day-old plants by RT-qPCR. Expression levels in the mutants are presented in relation to those in Col-0 or Ler (arbitrarily set to 1.0). Error bars indicate SDs of three biological replicates. Asterisks indicate significant differences between the indicated samples ($p < 0.05$, t test).

(E) Detection of the expression levels of AGO1-bound genes in 10-day-old ago1-36 complemented with wild-type AGO1 or one of the two mutant forms of AGO1 by RT-qPCR. #1 and #2 are independent transgenic lines. Expression levels in the mutant and transgenic lines are presented in relation to those in Col-0 (arbitrarily set to 1.0). At1g01540, a non-AGO1-bound gene, served as a negative control. Error bars indicate SDs of three biological replicates. Asterisks indicate significant differences between the indicated samples ($p < 0.05$, t test).

See also Figures S1 and S3 and Tables S1 and S2.

Next we sought to determine whether sRNAs are required for AGO1 binding to chromatin. The *Arabidopsis* genome encodes four DCL proteins that produce distinct sRNA species (Chapman and Carrington, 2007). As shown by our ChIP-qPCR results, AGO1 binding to its target genes was significantly compromised in *dcl1-9* and *dcl1/2/3/4* mutants but not in the *dcl2/3/4* mutant (Figure 4C), suggesting that DCL1-dependent sRNAs are required for AGO1 binding to its targets. Likely as a result of reduced AGO1 binding, the expression levels of the target genes were markedly decreased in *dcl1-9* and *dcl1/2/3/4* (Figure 4D). To examine whether these sRNAs are similar in biogenesis to miRNAs, the expression levels of nuclear AGO1 target genes were detected in the miRNA biogenesis mutant *hy1-2* (Kurihara et al., 2006; Vazquez et al., 2004) (Figure S3E). Opposite to the derepressed expression of miRNA target gene *ARF8*, the expression of eight out of nine nuclear AGO1 target genes was significantly decreased in *hy1-2* (Figure S3E), suggesting that nuclear AGO1-associated sRNAs could share the biogenesis machinery with miRNAs.

To further confirm that sRNAs play a role in directing AGO1 binding to chromatin, we examined the expression levels of AGO1 target genes in the *ago1-36* mutant complemented with wild-type AGO1 or two forms of mutated AGO1. The YF/AA form of AGO1 harbors alanine substitutions at two critical residues that are shown to be required for sRNA binding (Guang et al., 2008; Ma et al., 2004; Ye et al., 2012). The D848A form of AGO1 is able to bind sRNAs but is deficient in passenger strand removal due to its slicer deficiency (Iki et al., 2010; Ye et al., 2012). Both the YF/AA form and D848A form of AGO1 could not rescue the developmental phenotype of *ago1-36* (Figure S3F). We found that wild-type AGO1 readily restored the expression of nuclear AGO1-bound genes to normal levels but the YF/AA and D848A mutant forms of AGO1 could not (Figure 4E). Although failures of the YF/AA and D848A mutant forms of AGO1 to restore gene expression could arise from disruption of miRNA function and the resultant defects in plant development, such failures were most likely attributed to defects of these mutant forms in activation of gene transcription, because they were unable to restore the levels of nascent pre-mRNA transcripts (Figure S3H) and the transcription rates (Figure S3I) of nuclear AGO1-bound genes. Our ChIP-qPCR further revealed that these AGO1 mutants, compared with wild-type AGO1, had an abolished or greatly reduced capability for nuclear AGO1 target gene binding (Figure S3J). Altogether, our results indicate that sRNA binding and the formation of mature AGO1/sRNA complexes are required for AGO1 to bind to chromatin to regulate gene expression.

SWI/SNF Complexes Interact with AGO1 and Facilitate Its Binding to the Chromatin

In order to uncover factors involved in AGO1 binding to chromatin and promoting gene transcription, nuclear IgG and AGO1 immunoprecipitates (Figure S3A) were subjected to mass spectrometry analysis. Multiple potential binding partners of nuclear AGO1 were specifically identified in nuclear AGO1 immunoprecipitates (Table S3). Among the proteins that were identified, SWI3 proteins and BSH were of our great interest because they are core subunits of the SWI/SNF chromatin-remodeling complexes implicated in regulating chromatin accessibility and

gene transcription (Han et al., 2015; Jiang and Pugh, 2009). To confirm the interactions of AGO1 with SWI3 proteins and BSH, we transiently transfected *Arabidopsis* protoplasts with constructs expressing tagged proteins and then performed reciprocal co-immunoprecipitation. As expected, AGO1 could be co-immunoprecipitated with GFP-tagged SWI3B, SWI3D, and BSH, and vice versa (Figures 5A and S4A).

In plants, different combinations of SWI3 proteins and BSH associate with one of three types of SWI/SNF chromatin-remodeling ATPases called BRAHMA (BRM), SPLAYED (SYD), and MINUSCULE (MINU) as well as other accessory subunits to form SWI/SNF complexes (Han et al., 2015). To assess whether the SWI/SNF complexes play a role in nuclear AGO1 targeting, we first examined AGO1 binding to its target genes in two mutants for subunits of the SWI/SNF complexes *swi3b-2/+* (heterozygous for a null mutation of *SWI3B*) (Sarnowski et al., 2005) and *brm-4* (Tang et al., 2008) by ChIP-seq. We found that AGO1 binding to its targets was compromised genome-wide in *swi3b-2/+* and *brm-4* (Figure 5B). We then examined AGO1 binding to selected loci by ChIP-qPCR (Figure 5C). The *swi3b-2/+*, *swi3d-2* (Sarnowski et al., 2005), and *brm-4* mutations led to significant reduction of AGO1 binding at *At3g16240* and *At2g45180* (Figure 5C). At *At3g26520*, AGO1 binding was affected by the *swi3b-2/+*, *swi3d-2*, *brm-4*, and *syd-4* (Zhu et al., 2013) mutations (Figure 5C). We further performed RT-qPCR and found that the expression levels of *At3g16240*, *At2g45180*, and *At3g26520* were also decreased by different mutations (Figure 5D). The overall abundances and cytoplasmic/nuclear distribution of AGO1 were comparable in Col-0 and *swi3b-2/+* mutants, excluding the possibility that reduced expression or altered cytoplasmic/nuclear distribution of AGO1 contributed to the reduction in AGO1 binding and gene expression in the mutants (Figures S4B and S4C). These results together suggest that different SWI/SNF complexes are required for nuclear AGO1 targeting at different gene loci. We also tested the possibility that AGO1 is recruited to its target genes first and then it assists the targeting of the SWI/SNF complexes. However, our ChIP-qPCR results revealed that SWI3B enrichment at AGO1 target genes was not affected by the *ago1-36* mutation (Figure 5E), arguing against the possibility that AGO1 assists SWI3B recruitment.

Plant Hormones and Stresses Trigger AGO1 Binding to Stimuli-Responsive Genes

To understand the biological processes associated with nuclear AGO1-bound genes, all AGO1-bound genes were subjected to Gene Ontology (GO) analysis. Intriguingly, this showed a high enrichment for genes responding to different types of stimuli (Figure 6A and Table S4), suggesting that AGO1 may play an important role in responses to stimuli. We thus investigated whether AGO1 binding to genes is responsive to different stimuli, including plant hormones, biotic stresses, and abiotic stresses. We performed AGO1 ChIP-seq experiments using Col-0 seedlings that were mock treated or treated with methyl jasmonate (MeJA), indoleacetic acid (IAA), benzothiadiazole (BTH), flg22, or cold (Table S1). JA is a phytohormone that is perceived by its receptor, the F box protein Coronatine Insensitive 1 (COI1), which recruits JAZ repressors for degradation and thereby activates diverse JA responses (Song et al., 2014). IAA is perceived

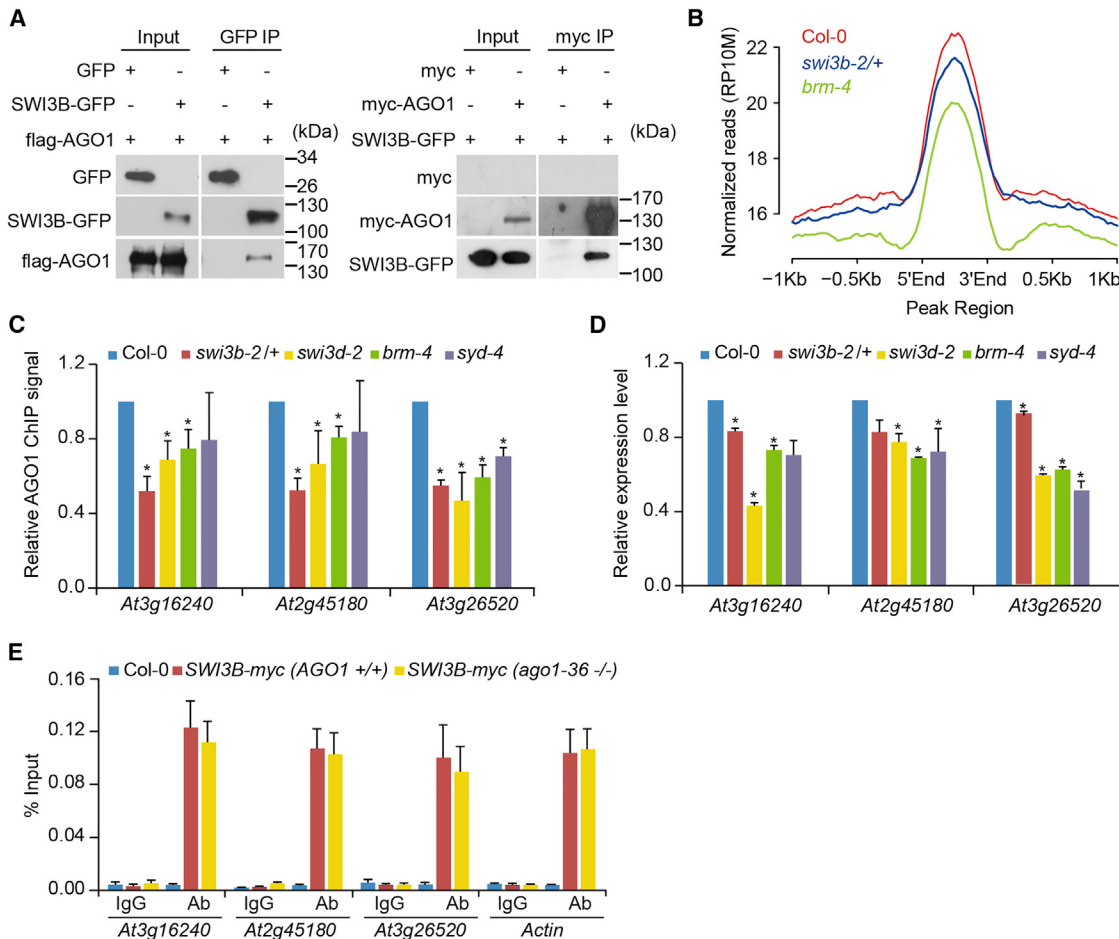


Figure 5. SWI/SNF Complexes Are Required for the Association of AGO1 with the Chromatin

(A) Detection of the interaction between AGO1 and SWI3B by co-immunoprecipitation. Tagged AGO1 and SWI3B were transiently expressed in *Arabidopsis* protoplasts and immunoprecipitated. Total extracts (Input) and the immunoprecipitates (IPs) were analyzed by western blot. The intensities of the bands were quantified and presented. The positions of molecular weight markers are shown on the right.

(B) A metaplot showing the distribution of AGO1 ChIP-seq reads as RP10M across AGO1-bound loci in 10-day-old Col-0, *swi3b-2/+*, and *brm-4* seedlings.

(C) Detection of AGO1 binding to AGO1 target genes in the indicated plants by ChIP-qPCR. AGO1 ChIP signals in the mutants are presented in relation to those in Col-0 (arbitrarily set to 1.0). Error bars indicate SDs of three biological replicates. Asterisks indicate significant differences between the indicated samples ($p < 0.05$, t test).

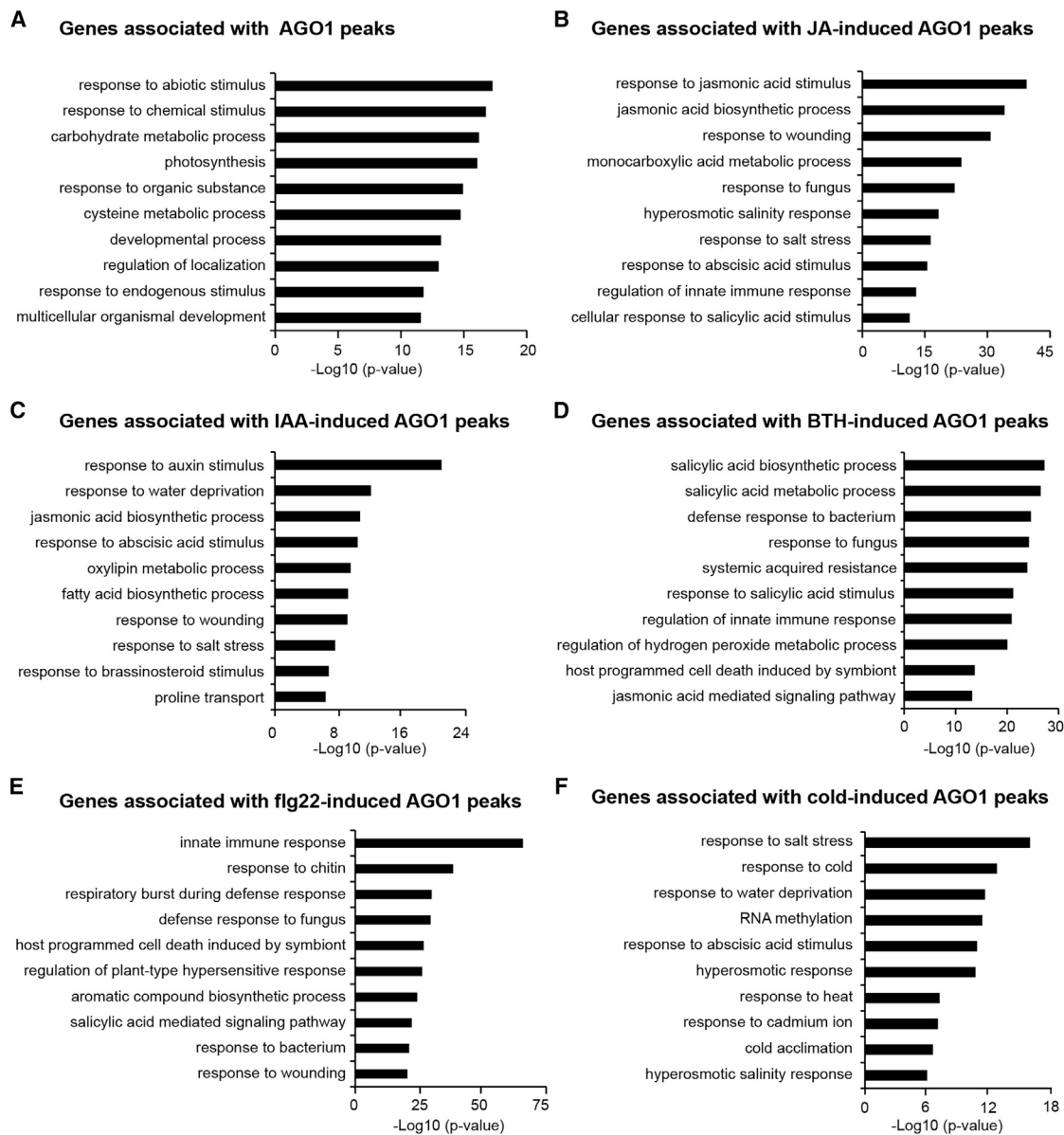
(D) Detection of the expression levels of AGO1 target genes in the indicated plants by RT-qPCR. Expression levels in the mutants are presented in relation to those in Col-0 (arbitrarily set to 1.0). Error bars indicate SDs of three biological replicates. Asterisks indicate significant differences between Col-0 and the indicated mutants ($p < 0.05$, t test).

(E) Detection of SWI3B binding to AGO1 target genes in Col-0 and the *pSWI3B:SWI3B-myc* transgenic plants in the *AGO1* (+/+) or *ago1-36* (-/-) mutant background. Error bars indicate SDs of three biological replicates. No significant difference was found between the *pSWI3B:SWI3B-myc* transgenic plants with and without AGO1 (t test).

See also Figure S4 and Tables S1, S2, and S3.

by a transient co-receptor complex consisting of a TIR1/AFB protein and an Aux/IAA protein. Auxin binding to the co-receptor results in degradation of the Aux/IAAs and de-repression of ARF-based transcription (Salehin et al., 2015). BTH is a chemical activator of systemic acquired resistance to diseases (Lawton et al., 1996). Flg22 is a peptide representing the elicitor-active epitope of flagellin and induces many defense-related genes (Zipfel et al., 2004). Cold stress is a major environmental factor that triggers the CBF/DREB-mediated transcriptional regulatory cascade, which is essential for the induction of a set of cold responsive (COR) genes (Shi et al., 2015).

Strikingly, we found that all treatments greatly increased the levels of AGO1 binding to some chromatic regions. Specifically, we identified 231, 338, 282, 1033, and 746 regions that had increased AGO1 binding upon treatment with MeJA, IAA, BTH, flg22, and cold treatment, respectively (Table S5 and Figures 7A and S5). Like AGO1 peaks under normal conditions, stimulus-induced AGO1 peaks were significantly over-represented within genic regions. Within genes, AGO1 was enriched throughout the genic sequences, with its enrichment highest near the TSS and the TTS, respectively (Figure S6). GO analyses revealed that genes associated with these induced peaks were strongly

**Figure 6. Gene Ontology Enrichment Analysis for the Genes Associated with Stimuli-Induced AGO1 Peaks**

(A–F) Top 10 GO biological process terms significantly enriched in genes associated with AGO1 peaks that were identified in *Arabidopsis* grown under normal conditions (A) or treated with MeJA (B), IAA (C), BTH (D), flg22 (E), and cold (F). See also Figures S5–S7 and Tables S1, S4, and S5.

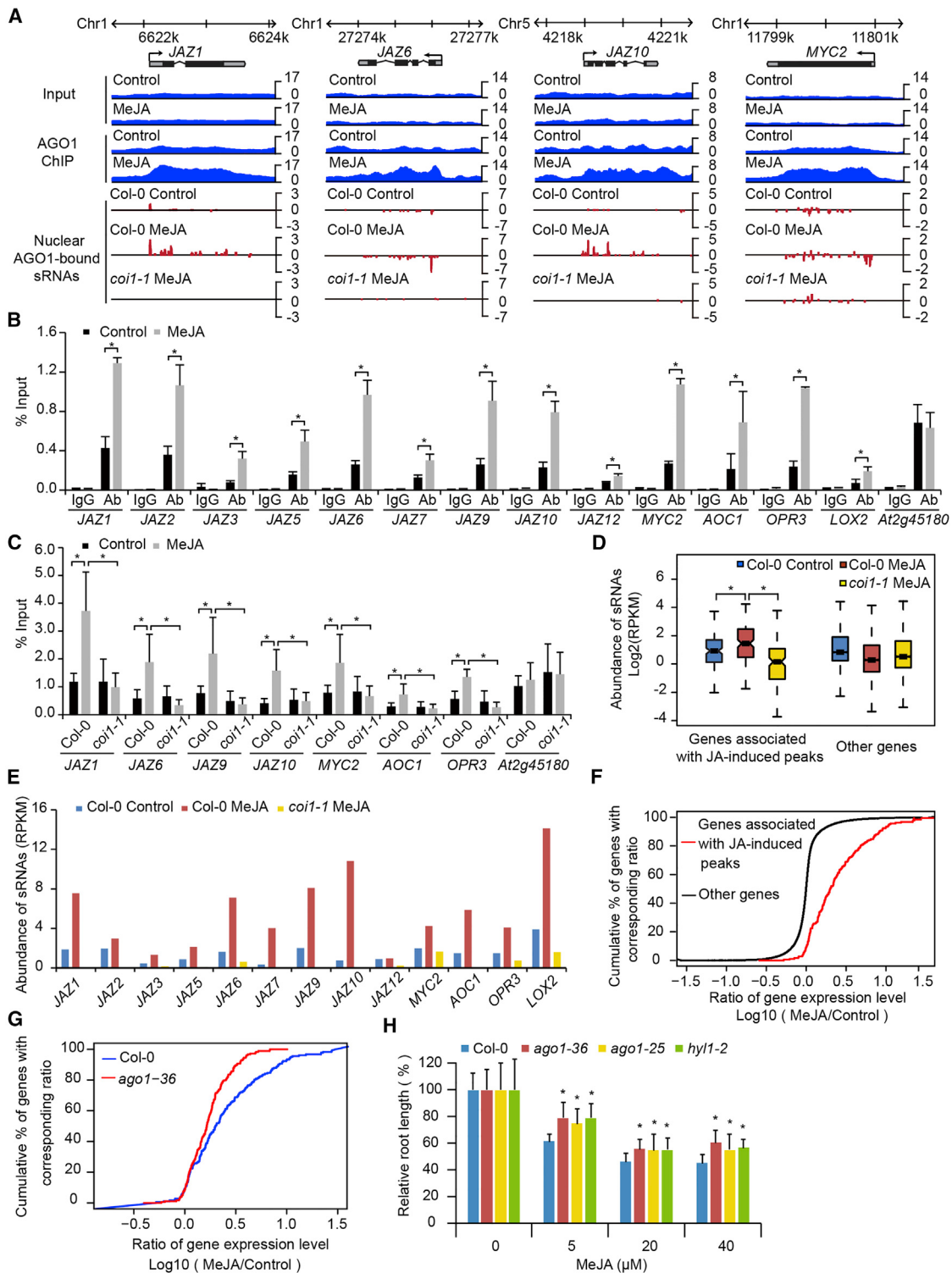
correlated with functions related to responses to the specific treatments (Figures 6B–6F and Table S4). The induction of AGO1 binding to selected gene loci by the treatments was confirmed by ChIP-qPCR (Figures 7B and S7A–S7D).

To gain more insights into the function of nuclear AGO1 in one particular signaling pathway, we narrowed our study down to the JA response. As shown in Figures 7A, 7B, and S5A, MeJA treatment induced AGO1 binding to genes implicated in the JA pathway, including *JAZ* family genes, *MYC2*, *LOX2*, and other genes (Bell et al., 1995; Dombrecht et al., 2007; Thines et al., 2007). However, such increases were not seen in the null mutant for the JA receptor COI1 (Yan et al., 2009) (Figure 7C), demon-

strating that the induction of AGO1 binding to its target genes is not an off-target effect.

We explored whether sRNAs were associated with MeJA-induced AGO1 binding. We analyzed sRNAs bound by nuclear AGO1 in plants treated with or without MeJA (Table S1). We found that MeJA treatment induced sRNA production from JA-responsive AGO1 target genes and sRNA production was abolished in the *coi1-1* mutant (Figures 7A, 7D, 7E, and S5A, and Table S5), hinting that sRNAs could be involved in MeJA-induced AGO1 binding.

We next investigated whether, as a consequence of AGO1 binding, genes associated with MeJA-induced peaks could

**Figure 7. Nuclear AGO1 Functions in the JA Signaling Pathway**

(A) Genome browser views of MeJA-induced AGO1 peaks and sRNAs bound by nuclear AGO1, with normalized read counts per million (RP) along the y axis.

(B) Validation of selected genes associated with MeJA-induced AGO1 peaks by ChIP-qPCR. ChIP was performed in 10-day-old plants without (Control) or with MeJA treatment. At2g45180, an AGO1-bound gene that is not induced by MeJA, was used as a control. Error bars indicate SDs of three biological replicates. Asterisks indicate significant differences between the indicated samples ($p < 0.05$, t test).

(C) Detection of AGO1 occupancy at the indicated genes in 10-day-old Col-0 and coi1-1 plants without (Control) or with MeJA treatment.

(legend continued on next page)

exhibit increased expression upon MeJA treatment by performing RNA-seq. We found that a significantly larger fraction of genes associated with MeJA-induced peaks had increased expression (Figure 7F and Table S5). This global induction was partially abolished in *ago1-36* (Figure 7G and Table S5), supporting that AGO1 contributes to the induction of gene expression by MeJA. Finally, to determine whether AGO1-mediated gene induction upon MeJA treatment has biological consequences, we tested the effect of AGO1 dysfunction on MeJA-induced root growth inhibition and found that MeJA-induced root growth inhibition was significantly alleviated in *ago1-36*, *ago1-25*, and *hy1-2* (Figure 7H). This result demonstrates the importance of AGO1 in the JA signaling pathway and, together with our other findings, hints that AGO1 may play a general role in many stimuli-related signaling pathways.

DISCUSSION

Arabidopsis AGO1 is known to bind miRNAs and repress gene expression at the post-transcriptional level. In this study, we demonstrate that AGO1 also binds to chromatin and promotes gene expression at the transcriptional level. AGO proteins have been shown to associate with chromatin and modulate gene expression at specific loci (Ameyar-Zazoua et al., 2012; Carissimi et al., 2015; Cernilgar et al., 2011; Huang et al., 2013; Taliaferro et al., 2013).

An important question in the studies of nuclear AGO proteins is how AGO proteins are targeted to achieve locus specificity. In human cancer cells, it has been proposed that miRNA mediates interactions of nuclear AGO1 with chromatin and RNAP II (Huang et al., 2013). Here, we provide evidence demonstrating that nuclear AGO1 in *Arabidopsis* needs to bind to sRNAs for site-specific targeting. DCL1, which generated 21-nt sRNAs, is required for AGO1 binding to its target genes and AGO1-mediated gene activation (Figures 4C and 4D). The two mutant forms of AGO1, one deficient in sRNA binding and the other deficient in slicing and forming mature AGO1/sRNA complex, are unable to activate the expression of genes targeted by nuclear AGO1 (Figure 4E). AGO1-bound genes do not have putative target sites of known miRNAs (data not shown), indicating that AGO1 binding is unlikely mediated by miRNAs. Interestingly, we found that 55% of the AGO1 target genes produce 21-nt sRNAs bound to nuclear AGO1 (Figures 4A and 4B, and Table S2). It should be noted that this percentage could be underestimated due to our relatively low sequencing depth (<10 million). We propose that

these sRNAs, which appear to share the biogenesis machinery with miRNAs, are guides for AGO1 to bind its targets.

The nuclear AGO1-associated sRNAs are reminiscent of AGO2-associated sRNAs enriched in the promoter regions of the *Drosophila* genome in that they both contribute to transcriptional regulation (Cernilgar et al., 2011). However, AGO2-dependent sRNAs in *Drosophila* appear to interfere with gene transcription, especially under heat-shocked conditions (Cernilgar et al., 2011). The nuclear AGO1-associated sRNAs also resemble sRNAs arising from SWI/SNF bound TSSs (swiRNAs) that are bound to AGO2 and mapped near the TSS occupied by the SWI/SNF complexes in human cells, but it seems that swiRNAs merely regulate nucleosome occupancy without influencing gene expression (Carissimi et al., 2015).

Apart from sRNAs, we found that components in the SWI/SNF complexes interact with nuclear AGO1 (Figures 5A and S4A, and Table S3) and are required for AGO1 binding to target genes (Figures 5B and 5C). Our results, together with previous finding that AGO2 cooperates with the SWI/SNF complexes to regulate nucleosome positioning in human cells (Carissimi et al., 2015), suggest that the SWI/SNF complexes may play a conserved role in recruiting AGO proteins in plants and humans. In addition to the components of the SWI/SNF complexes, our mass spectrometry analysis of nuclear AGO1-associated proteins identified several subunits of the Mediator complex (Table S3), which serves as a platform for the recruitment of Pol II, general transcriptional factors, and other cofactors to form a functional pre-initiation complex (Conaway and Conaway, 2011; Dolan and Chapple, 2016). Further investigation is needed to determine whether the Mediator complex participates in the recruitment of AGO1 to specific gene loci or the other way around.

We demonstrated that chromatin-bound AGO1 promotes gene expression at the transcriptional level. However, a question emerges as to how AGO1 promotes gene transcription. We found that Pol II occupancy at AGO1 target genes, irrespective of its phosphorylation status, is greatly reduced by AGO1 depletion (Figures 3C and S2), suggesting that AGO1 may promote gene transcription through facilitating the recruitment of Pol II. In support, key subunits of Pol II were identified in the nuclear AGO1 immunoprecipitates (Table S3), and the patterns of AGO1 and Pol II distribution on AGO1 target genes were nearly identical (compare Figure 1E with Figure 3C). The association of AGO proteins and the core transcriptional machinery has

(D) Box plots showing the abundances of nuclear AGO1-bound sRNAs produced from genes associated with MeJA-induced AGO1 peaks. Genes not associated with MeJA-induced AGO1 peaks (Other genes) were used as controls. Asterisks indicate significant differences between the indicated groups (two-sided Wilcoxon test, $p < 0.01$).

(E) Abundances of nuclear AGO1-bound sRNAs mapped to the indicated genes.

(F) Cumulative distribution plots of fold change of expression for genes associated with MeJA-induced AGO1 peaks and for those not associated with MeJA-induced peaks (other genes) in Col-0. The x axis represents log₁₀-transformed fold change in gene expression between MeJA treatment and the control treatment.

(G) Cumulative distribution plots of fold change of expression for genes associated with MeJA-induced AGO1 peaks in Col-0 and *ago1-36*. The x axis represents log₁₀-transformed fold change in gene expression between MeJA treatment and the control treatment.

(H) Root growth inhibition assay of 10-day-old Col-0, *ago1-36*, *ago1-25*, and *hy1-2* seedlings. Plants were grown on 1/2 strength Murashige and Skoog medium containing the indicated concentrations of MeJA. The root measurements for all treatments were normalized with those under the mock condition. Results shown are the mean of more than 20 seedlings at each concentration. Error bars indicate SDs. Asterisks indicate significant differences between Col-0 and *ago1-36* ($p < 0.05$, t test).

See also Figure S5 and Tables S1 and S5.

been observed in *Drosophila* and human cells (Ameyar-Zazoua et al., 2012; Cernilgar et al., 2011; Huang et al., 2013; Taliaferro et al., 2013), suggesting that AGO proteins are physically and functionally coupled to the transcriptional machinery across various organisms. Interactions of nuclear AGO1 with the subunits of the SWI/SNF complexes and the Mediator complex lead us to speculate that these two complexes may be also involved in determining the activating role of AGO1. The SWI/SNF complexes often associate with activating chromatin regulators to increase chromatin accessibility (Han et al., 2015) and the Mediator complex is well known for its role in enhancing basal and activator-dependent transcription (Samanta and Thakur, 2015).

The biological significance of AGO1's role in activating gene expression is underscored by our findings that AGO1 binding to chromatin is responsive to hormonal, biotic, and abiotic stresses (Figures 6 and 7). The SWI/SNF complexes, which were found to recruit AGO1 (Figures 5 and S4), have been shown to regulate gene expression during *Arabidopsis* development (Sarnowski et al., 2005) and in plant responses to hormonal, biotic, and abiotic stimuli (Buszewicz et al., 2016; Jegu et al., 2015; Peirats-Llobet et al., 2016; Saez et al., 2008; Walley et al., 2008). This is in accordance with our findings that AGO1 also plays an important regulatory role in multiple stimuli-related signaling pathways and further suggests that the effects of AGO1 on gene expression are specific. The association of AGO1 with the transcriptional machinery and the chromatin of stimuli-responsive genes in multiple signaling pathways leads us to propose that AGO1 could integrate input from distinct signaling pathways.

STAR★METHODS

Detailed methods are provided in the online version of this paper and include the following:

- KEY RESOURCES TABLE
- CONTACT FOR REAGENT AND RESOURCE SHARING
- EXPERIMENTAL MODEL AND SUBJECT DETAILS
- METHOD DETAILS
 - DNA Constructs and Plant Transformation
 - Protoplast Transfection
 - Confocal Fluorescence Microscopy
 - Subcellular Fractionation
 - Chromatin Immunoprecipitation
 - ChIP Sequencing Analysis
 - RNA Sequencing Analysis
 - Quantitative PCR
 - Nuclear Run-On
 - Global Run-On Sequencing Analysis
 - Identification of Small RNAs and Proteins Associated with Nuclear AGO1
 - Gene Ontology Analysis
 - Generation of the Control Gene Sets
 - Co-immunoprecipitation
 - Western Blot Analysis
 - Root Measurement
- QUANTIFICATION AND STATISTICAL ANALYSIS
- DATA AND SOFTWARE AVAILABILITY

SUPPLEMENTAL INFORMATION

Supplemental Information includes seven figures and six tables and can be found with this article online at <https://doi.org/10.1016/j.devcel.2017.12.002>.

ACKNOWLEDGMENTS

We are grateful to Drs. Jianmin Zhou, Shuhua Yang, Yan Guo, and Lijia Qu for help with plant hormone and stress treatments. This work was funded by grants from the National Natural Science Foundation of China (grant nos. 31330042 and 31421001) and the Ministry of Science and Technology of China (grant no. 2016YFA0500800) to Y.Q. Y.Q. is a visiting investigator of the CAS Center for Excellence in Molecular Plant Sciences.

AUTHOR CONTRIBUTIONS

C.L. and Y.Q. designed the experiments; C.L., Y. Xin, L.X., Z.C., and Y. Xue conducted the experiments; C.L., Y. Xin, L.X., D.X., Yule Liu, Yong Liu, and Y.Q. analyzed the data; Y.Q. wrote the paper.

DECLARATION OF INTERESTS

The authors declare no competing interests.

Received: May 6, 2017

Revised: November 22, 2017

Accepted: December 1, 2017

Published: December 28, 2017

REFERENCES

- Adelman, K., and Lis, J.T. (2012). Promoter-proximal pausing of RNA polymerase II: emerging roles in metazoans. *Nat. Rev. Genet.* 13, 720–731.
- Ameyar-Zazoua, M., Rachez, C., Souidi, M., Robin, P., Fritsch, L., Young, R., Morozova, N., Fenouil, R., Descostes, N., Andrau, J.C., et al. (2012). Argonaute proteins couple chromatin silencing to alternative splicing. *Nat. Struct. Mol. Biol.* 19, 998–1004.
- Aravin, A.A., Hannon, G.J., and Brennecke, J. (2007). The Piwi-piRNA pathway provides an adaptive defense in the transposon arms race. *Science* 318, 761–764.
- Baulcombe, D. (2004). RNA silencing in plants. *Nature* 431, 356–363.
- Baumberger, N., and Baulcombe, D.C. (2005). *Arabidopsis ARGONAUTE1* is an RNA Slicer that selectively recruits microRNAs and short interfering RNAs. *Proc. Natl. Acad. Sci. USA* 102, 11928–11933.
- Bell, E., Creelman, R.A., and Mullet, J.E. (1995). A chloroplast lipoxygenase is required for wound-induced jasmonic acid accumulation in *Arabidopsis*. *Proc. Natl. Acad. Sci. USA* 92, 8675–8679.
- Bohmert, K., Camus, I., Bellini, C., Bouchez, D., Caboche, M., and Benning, C. (1998). AGO1 defines a novel locus of *Arabidopsis* controlling leaf development. *EMBO J.* 17, 170–180.
- Buszewicz, D., Archacki, R., Palusinski, A., Kotlinski, M., Fogtman, A., Iwanicka-Nowicka, R., Sosnowska, K., Kucinski, J., Pupel, P., Oledzki, J., et al. (2016). HD2C histone deacetylase and a SWI/SNF chromatin remodeling complex interact and both are involved in mediating the heat stress response in *Arabidopsis*. *Plant Cell Environ.* 39, 2108–2122.
- Carissimi, C., Laudadio, I., Cipolletta, E., Gioiosa, S., Mihailovich, M., Bonaldi, T., Macino, G., and Fulci, V. (2015). ARGONAUTE2 cooperates with SWI/SNF complex to determine nucleosome occupancy at human Transcription Start Sites. *Nucleic Acids Res.* 43, 1498–1512.
- Cernilgar, F.M., Onorati, M.C., Kothe, G.O., Burroughs, A.M., Parsi, K.M., Breiling, A., Lo Sardo, F., Saxena, A., Miyoshi, K., Siomi, H., et al. (2011). Chromatin-associated RNA interference components contribute to transcriptional regulation in *Drosophila*. *Nature* 480, 391–395.
- Chapman, E.J., and Carrington, J.C. (2007). Specialization and evolution of endogenous small RNA pathways. *Nat. Rev. Genet.* 8, 884–896.

- Clough, S.J., and Bent, A.F. (1998). Floral dip: a simplified method for *Agrobacterium*-mediated transformation of *Arabidopsis thaliana*. *Plant J.* 16, 735–743.
- Conaway, R.C., and Conaway, J.W. (2011). Function and regulation of the Mediator complex. *Curr. Opin. Genet. Dev.* 21, 225–230.
- Conine, C.C., Moresco, J.J., Gu, W., Shirayama, M., Conte, D., Jr., Yates, J.R., 3rd, and Mello, C.C. (2013). Argonautes promote male fertility and provide a paternal memory of germline gene expression in *C. elegans*. *Cell* 155, 1532–1544.
- Core, L.J., Waterfall, J.J., and Lis, J.T. (2008). Nascent RNA sequencing reveals widespread pausing and divergent initiation at human promoters. *Science* 322, 1845–1848.
- Curtis, M.D., and Grossniklaus, U. (2003). A gateway cloning vector set for high-throughput functional analysis of genes in planta. *Plant Physiol.* 133, 462–469.
- Dolan, W.L., and Chapple, C. (2016). Conservation and divergence of mediator structure and function: insights from plants. *Plant Cell Physiol.* 58, 4–21.
- Dolata, J., Bajczyk, M., Bielewicz, D., Niedojadlo, K., Niedojadlo, J., Pietrykowska, H., Walczak, W., Szwejkowska-Kulinska, Z., and Jarmolowski, A. (2016). Salt stress reveals a new role for ARGONAUTE1 in miRNA biogenesis at the transcriptional and posttranscriptional levels. *Plant Physiol.* 172, 297–312.
- Dombrecht, B., Xue, G.P., Sprague, S.J., Kirkegaard, J.A., Ross, J.J., Reid, J.B., Fitt, G.P., Sewelam, N., Schenk, P.M., Manners, J.M., et al. (2007). MYC2 differentially modulates diverse jasmonate-dependent functions in *Arabidopsis*. *Plant Cell* 19, 2225–2245.
- Du, Z., Zhou, X., Ling, Y., Zhang, Z., and Su, Z. (2010). agriGO: a GO analysis toolkit for the agricultural community. *Nucleic Acids Res.* 38, W64–W70.
- Earley, K.W., Haag, J.R., Pontes, O., Opper, K., Juehne, T., Song, K., and Pikaard, C.S. (2006). Gateway-compatible vectors for plant functional genomics and proteomics. *Plant J.* 45, 616–629.
- Fang, X., Cui, Y., Li, Y., and Qi, Y. (2015). Transcription and processing of primary microRNAs are coupled by Elongator complex in *Arabidopsis*. *Nat. Plants* 1, 15075.
- Fang, X., and Qi, Y. (2016). RNAi in plants: an Argonaute-centered view. *Plant Cell* 28, 272–285.
- Fang, Y., and Spector, D.L. (2007). Identification of nuclear dicing bodies containing proteins for microRNA biogenesis in living *Arabidopsis* plants. *Curr. Biol.* 17, 818–823.
- Guang, S., Bochner, A.F., Pavlak, D.M., Burkhardt, K.B., Harding, S., Lachowicz, J., and Kennedy, S. (2008). An Argonaute transports siRNAs from the cytoplasm to the nucleus. *Science* 321, 537–541.
- Hajheidari, M., Koncz, C., and Eick, D. (2013). Emerging roles for RNA polymerase II CTD in *Arabidopsis*. *Trends Plant Sci.* 18, 633–643.
- Han, S.K., Wu, M.F., Cui, S., and Wagner, D. (2015). Roles and activities of chromatin remodeling ATPases in plants. *Plant J.* 83, 62–77.
- Heidemann, M., Hintermair, C., Voss, K., and Eick, D. (2013). Dynamic phosphorylation patterns of RNA polymerase II CTD during transcription. *Biochim. Biophys. Acta* 1829, 55–62.
- Heinz, S., Benner, C., Spann, N., Bertolino, E., Lin, Y.C., Laslo, P., Cheng, J.X., Murre, C., Singh, H., and Glass, C.K. (2010). Simple combinations of lineage-determining transcription factors prime cis-regulatory elements required for macrophage and B cell identities. *Mol. Cell* 38, 576–589.
- Henderson, I.R., Zhang, X., Lu, C., Johnson, L., Meyers, B.C., Green, P.J., and Jacobsen, S.E. (2006). Dissecting *Arabidopsis thaliana* DICER function in small RNA processing, gene silencing and DNA methylation patterning. *Nat. Genet.* 38, 721–725.
- Hetzell, J., Duttke, S.H., Benner, C., and Chory, J. (2016). Nascent RNA sequencing reveals distinct features in plant transcription. *Proc. Natl. Acad. Sci. USA* 113, 12316–12321.
- Huang, V., Zheng, J., Qi, Z., Wang, J., Place, R.F., Yu, J., Li, H., and Li, L.C. (2013). Ago1 interacts with RNA polymerase II and binds to the promoters of actively transcribed genes in human cancer cells. *PLoS Genet.* 9, e1003821.
- Iki, T., Yoshikawa, M., Nishikiori, M., Jaudal, M.C., Matsumoto-Yokoyama, E., Mitsuhashi, I., Meshi, T., and Ishikawa, M. (2010). In vitro assembly of plant RNA-induced silencing complexes facilitated by molecular chaperone HSP90. *Mol. Cell* 39, 282–291.
- Iwasaki, Y.W., Siomi, M.C., and Siomi, H. (2015). PIWI-interacting RNA: its biogenesis and functions. *Annu. Rev. Biochem.* 84, 405–433.
- Jacobsen, S.E., Running, M.P., and Meyerowitz, E.M. (1999). Disruption of an RNA helicase/RNase III gene in *Arabidopsis* causes unregulated cell division in floral meristems. *Development* 126, 5231–5243.
- Jegu, T., Domenichini, S., Blein, T., Ariel, F., Christ, A., Kim, S.K., Crespi, M., Boutet-Mercey, S., Mouille, G., Bourge, M., et al. (2015). A SWI/SNF chromatin remodelling protein controls cytokinin production through the regulation of chromatin architecture. *PLoS One* 10, e0138276.
- Jiang, C., and Pugh, B.F. (2009). Nucleosome positioning and gene regulation: advances through genomics. *Nat. Rev. Genet.* 10, 161–172.
- Joshua-Tor, L., and Hannon, G.J. (2011). Ancestral roles of small RNAs: an Ago-centric perspective. *Cold Spring Harb. Perspect. Biol.* 3, a003772.
- Kim, V.N. (2005). Small RNAs: classification, biogenesis, and function. *Mol. Cells* 19, 1–15.
- Kurihara, Y., Takashi, Y., and Watanabe, Y. (2006). The interaction between DCL1 and HYL1 is important for efficient and precise processing of pri-miRNA in plant microRNA biogenesis. *RNA* 12, 206–212.
- Langmead, B., Trapnell, C., Pop, M., and Salzberg, S.L. (2009). Ultrafast and memory-efficient alignment of short DNA sequences to the human genome. *Genome Biol.* 10, R25.
- Law, J.A., and Jacobsen, S.E. (2010). Establishing, maintaining and modifying DNA methylation patterns in plants and animals. *Nat. Rev. Genet.* 11, 204–220.
- Lawton, K.A., Friedrich, L., Hunt, M., Weymann, K., Delaney, T., Kessmann, H., Staub, T., and Ryals, J. (1996). Benzothiadiazole induces disease resistance in *Arabidopsis* by activation of the systemic acquired resistance signal transduction pathway. *Plant J.* 10, 71–82.
- Li, H., Handsaker, B., Wysoker, A., Fennell, T., Ruan, J., Homer, N., Marth, G., Abecasis, G., Durbin, R., and Genome Project Data Processing, S. (2009). The Sequence Alignment/Map format and SAMtools. *Bioinformatics* 25, 2078–2079.
- Liu, Z.W., Shao, C.R., Zhang, C.J., Zhou, J.X., Zhang, S.W., Li, L., Chen, S., Huang, H.W., Cai, T., and He, X.J. (2014). The SET domain proteins SUVH2 and SUVH9 are required for Pol V occupancy at RNA-directed DNA methylation loci. *PLoS Genet.* 10, e1003948.
- Ma, J.B., Ye, K., and Patel, D.J. (2004). Structural basis for overhang-specific small interfering RNA recognition by the PAZ domain. *Nature* 429, 318–322.
- Martenssen, R., and Moazed, D. (2015). RNAi and heterochromatin assembly. *Cold Spring Harb. Perspect. Biol.* 7, a019323.
- Matzke, M.A., and Mosher, R.A. (2014). RNA-directed DNA methylation: an epigenetic pathway of increasing complexity. *Nat. Rev. Genet.* 15, 394–408.
- Meister, G. (2013). Argonaute proteins: functional insights and emerging roles. *Nat. Rev. Genet.* 14, 447–459.
- Mi, S., Cai, T., Hu, Y., Chen, Y., Hodges, E., Ni, F., Wu, L., Li, S., Zhou, H., Long, C., et al. (2008). Sorting of small RNAs into *Arabidopsis* Argonaute complexes is directed by the 5' terminal nucleotide. *Cell* 133, 116–127.
- Montgomery, T.A., Howell, M.D., Cuperus, J.T., Li, D., Hansen, J.E., Alexander, A.L., Chapman, E.J., Fahlgren, N., Allen, E., and Carrington, J.C. (2008). Specificity of ARGONAUTE7-miR390 interaction and dual functionality in TAS3 trans-acting siRNA formation. *Cell* 133, 128–141.
- Morel, J.B., Godon, C., Mourrain, P., Beclin, C., Boutet, S., Feuerbach, F., Proux, F., and Vaucheret, H. (2002). Fertile hypomorphic ARGONAUTE (ago1) mutants impaired in post-transcriptional gene silencing and virus resistance. *Plant Cell* 14, 629–639.
- Moshkovich, N., Nisha, P., Boyle, P.J., Thompson, B.A., Dale, R.K., and Lei, E.P. (2011). RNAi-independent role for Argonaute2 in CTCF/CP190 chromatin insulator function. *Genes Dev.* 25, 1686–1701.
- Pearats-Llobet, M., Han, S.K., Gonzalez-Guzman, M., Jeong, C.W., Rodriguez, L., Belda-Palazon, B., Wagner, D., and Rodriguez, P.L. (2016). A direct link

- between abscisic acid sensing and the chromatin-remodeling ATPase BRAHMA via core ABA signaling pathway components. *Mol. Plant* 9, 136–147.
- Qi, Y., Denli, A.M., and Hannon, G.J. (2005). Biochemical specialization within *Arabidopsis* RNA silencing pathways. *Mol. Cell* 19, 421–428.
- R Core Team. (2014). R: A Language and Environment for Statistical Computing (R Foundation for Statistical Computing).
- Roberts, T.C., Hart, J.R., Kaikkonen, M.U., Weinberg, M.S., Vogt, P.K., and Morris, K.V. (2015). Quantification of nascent transcription by bromouridine immunocapture nuclear run-on RT-qPCR. *Nat. Protoc.* 10, 1198–1211.
- Rogers, K., and Chen, X. (2013). Biogenesis, turnover, and mode of action of plant microRNAs. *Plant Cell* 25, 2383–2399.
- Saez, A., Rodrigues, A., Santiago, J., Rubio, S., and Rodriguez, P.L. (2008). HAB1-SWI3B interaction reveals a link between abscisic acid signaling and putative SWI/SNF chromatin-remodeling complexes in *Arabidopsis*. *Plant Cell* 20, 2972–2988.
- Salehin, M., Bagchi, R., and Estelle, M. (2015). SCFTIR1/AFB-based auxin perception: mechanism and role in plant growth and development. *Plant Cell* 27, 9–19.
- Samanta, S., and Thakur, J.K. (2015). Importance of Mediator complex in the regulation and integration of diverse signaling pathways in plants. *Front. Plant Sci.* 6, 757.
- Sarnowski, T.J., Rios, G., Jasik, J., Swiezewski, S., Kaczanowski, S., Li, Y., Kwiatkowska, A., Pawlikowska, K., Kozbial, M., Kozbial, P., et al. (2005). SWI3 subunits of putative SWI/SNF chromatin-remodeling complexes play distinct roles during *Arabidopsis* development. *Plant Cell* 17, 2454–2472.
- Seth, M., Shirayama, M., Gu, W., Ishidate, T., Conte, D., Jr., and Mello, C.C. (2013). The *C. elegans* CSR-1 Argonaute pathway counteracts epigenetic silencing to promote germline gene expression. *Dev. Cell* 27, 656–663.
- Shen, L., Shao, N., Liu, X., and Nestler, E. (2014). ngs.plot: quick mining and visualization of next-generation sequencing data by integrating genomic databases. *BMC Genomics* 15, 284.
- Shi, Y., Ding, Y., and Yang, S. (2015). Cold signal transduction and its interplay with phytohormones during cold acclimation. *Plant Cell Physiol.* 56, 7–15.
- Song, S., Qi, T., Wasternack, C., and Xie, D. (2014). Jasmonate signaling and crosstalk with gibberellin and ethylene. *Curr. Opin. Plant Biol.* 21, 112–119.
- Taliaferro, J.M., Aspden, J.L., Bradley, T., Marwha, D., Blanchette, M., and Rio, D.C. (2013). Two new and distinct roles for *Drosophila* Argonaute-2 in the nucleus: alternative pre-mRNA splicing and transcriptional repression. *Genes Dev.* 27, 378–389.
- Tang, X., Hou, A., Babu, M., Nguyen, V., Hurtado, L., Lu, Q., Reyes, J.C., Wang, A., Keller, W.A., Harada, J.J., et al. (2008). The *Arabidopsis* BRAHMA chromatin-remodeling ATPase is involved in repression of seed maturation genes in leaves. *Plant Physiol.* 147, 1143–1157.
- Thines, B., Katsir, L., Melotto, M., Niu, Y., Mandaokar, A., Liu, G., Nomura, K., He, S.Y., Howe, G.A., and Browse, J. (2007). JAZ repressor proteins are targets of the SCF(CO11) complex during jasmonate signalling. *Nature* 448, 661–665.
- Trapnell, C., Pachter, L., and Salzberg, S.L. (2009). TopHat: discovering splice junctions with RNA-Seq. *Bioinformatics* 25, 1105–1111.
- Trapnell, C., Roberts, A., Goff, L., Pertea, G., Kim, D., Kelley, D.R., Pimentel, H., Salzberg, S.L., Rinn, J.L., and Pachter, L. (2012). Differential gene and transcript expression analysis of RNA-seq experiments with TopHat and Cufflinks. *Nat. Protoc.* 7, 562–578.
- Vazquez, F., Gasciolli, V., Crete, P., and Vaucheret, H. (2004). The nuclear dsRNA binding protein HYL1 is required for microRNA accumulation and plant development, but not posttranscriptional transgene silencing. *Curr. Biol.* 14, 346–351.
- Voinnet, O. (2009). Origin, biogenesis, and activity of plant microRNAs. *Cell* 136, 669–687.
- Volpe, T., and Martienssen, R.A. (2011). RNA interference and heterochromatin assembly. *Cold Spring Harb. Perspect. Biol.* 3, a003731.
- Walley, J.W., Rowe, H.C., Xiao, Y., Chehab, E.W., Kliebenstein, D.J., Wagner, D., and Dehesh, K. (2008). The chromatin remodeler SPLAYED regulates specific stress signaling pathways. *PLoS Pathog.* 4, e1000237.
- Wang, D., Garcia-Bassets, I., Benner, C., Li, W., Su, X., Zhou, Y., Qiu, J., Liu, W., Kaikkonen, M.U., Ohgi, K.A., et al. (2011a). Reprogramming transcription by distinct classes of enhancers functionally defined by eRNA. *Nature* 474, 390–394.
- Wang, W., Ye, R., Xin, Y., Fang, X., Li, C., Shi, H., Zhou, X., and Qi, Y. (2011b). An importin beta protein negatively regulates MicroRNA activity in *Arabidopsis*. *Plant Cell* 23, 3565–3576.
- Wendte, J.M., and Pikaard, C.S. (2017). The RNAs of RNA-directed DNA methylation. *Biochim. Biophys. Acta* 1860, 140–148.
- Yan, J., Zhang, C., Gu, M., Bai, Z., Zhang, W., Qi, T., Cheng, Z., Peng, W., Luo, H., Nan, F., et al. (2009). The *Arabidopsis* CORONATINE INSENSITIVE1 protein is a jasmonate receptor. *Plant Cell* 21, 2220–2236.
- Ye, R., Chen, Z., Lian, B., Rowley, M.J., Xia, N., Chai, J., Li, Y., He, X.J., Wierzbicki, A.T., and Qi, Y. (2016). A dicer-independent route for biogenesis of siRNAs that direct DNA methylation in *Arabidopsis*. *Mol. Cell* 61, 222–235.
- Ye, R., Wang, W., Iki, T., Liu, C., Wu, Y., Ishikawa, M., Zhou, X., and Qi, Y. (2012). Cytoplasmic assembly and selective nuclear import of *Arabidopsis* Argonaute4/siRNA complexes. *Mol. Cell* 46, 859–870.
- Yoo, S.D., Cho, Y.H., and Sheen, J. (2007). *Arabidopsis* mesophyll protoplasts: a versatile cell system for transient gene expression analysis. *Nat. Protoc.* 2, 1565–1572.
- Zhang, H., Tang, K., Qian, W., Duan, C.G., Wang, B., Zhang, H., Wang, P., Zhu, X., Lang, Z., Yang, Y., et al. (2014). An Rrp6-like protein positively regulates noncoding RNA levels and DNA methylation in *Arabidopsis*. *Mol. Cell* 54, 418–430.
- Zhang, H., and Zhu, J.K. (2011). RNA-directed DNA methylation. *Curr. Opin. Plant Biol.* 14, 142–147.
- Zhang, Y., Liu, T., Meyer, C.A., Eeckhoute, J., Johnson, D.S., Bernstein, B.E., Nusbaum, C., Myers, R.M., Brown, M., Li, W., et al. (2008). Model-based analysis of ChIP-Seq (MACS). *Genome Biol.* 9, R137.
- Zhu, Y., Rowley, M.J., Bohmdorfer, G., and Wierzbicki, A.T. (2013). A SWI/SNF chromatin-remodeling complex acts in noncoding RNA-mediated transcriptional silencing. *Mol. Cell* 49, 298–309.
- Zipfel, C., Robatzek, S., Navarro, L., Oakeley, E.J., Jones, J.D., Felix, G., and Boller, T. (2004). Bacterial disease resistance in *Arabidopsis* through flagellin perception. *Nature* 428, 764–767.

STAR★METHODS

KEY RESOURCES TABLE

REAGENT or RESOURCE	SOURCE	IDENTIFIER
Antibodies		
Rabbit polyclonal anti-AGO1	Qi et al., 2005	N/A
Rabbit polyclonal anti-PEP Carboxylase antibody	Abcam	Cat#ab34793; RRID: AB_777192
Mouse monoclonal anti- α -Tubulin [B-5-1-2]	Sigma-Aldrich	Cat#T5168; RRID: AB_477579
Rabbit polyclonal anti-Histone H3	Sigma-Aldrich	Cat# H0164; RRID: AB_532248
Mouse monoclonal anti-Pol II [8WG16]	Abcam	Cat#ab817; RRID: AB_306327
Mouse monoclonal anti Pol II Ser5P [H14]	Abcam	Cat#ab24759; RRID: AB_2167350
Mouse monoclonal anti Pol II Ser2P [H5]	Abcam	Cat#ab24758; RRID: AB_2167352
Sheep polyclonal anti-BrdU	Abcam	Cat#ab1893; RRID: AB_302659
Mouse monoclonal anti-GFP [mixture of two clones (7.1 and 13.1)]	Roche	Cat#11814460001; RRID: AB_390913
Mouse monoclonal anti-myc [9E10]	Abcam	Cat#ab32; RRID: AB_303599
Mouse monoclonal anti-c-myc [clone 9E10]	Roche	11667203001; RRID: AB_390911
Mouse monoclonal anti-flag [clone M2]	Sigma-Aldrich	F1804; RRID: AB_262044
Goat polyclonal anti-Mouse IgG (whole molecule)	Sigma-Aldrich	A4416; RRID: AB_258167
Goat polyclonal anti-Rabbit IgG (whole molecule)	Sigma-Aldrich	A0545; RRID: AB_257896
Rabbit IgG	Abmart	Cat#B30011
Mouse IgG	Abmart	Cat#B30010
Bacterial and Virus Strains		
<i>E. coli</i> DB3.1	N/A	N/A
<i>E. coli</i> DH5 α	N/A	N/A
<i>Agrobacterium tumefaciens</i> GV3101	N/A	N/A
Chemicals, Peptides, and Recombinant Proteins		
IAA	Sigma-Aldrich	Cat#I2886
MeJA	Sigma-Aldrich	Cat#392707
Benzothiadiazole	Sigma-Aldrich	Cat#B10900
Sarkosyl	Sigma-Aldrich	Cat#61747
5-bromo UTP	Sigma-Aldrich	Cat#B7166
TRIzol Reagent	Invitrogen	Cat#15596018
Yeast tRNA	Invitrogen	Cat#AM7119
RNase inhibitor	Promega	Cat#N2515
Protease inhibitor cocktail	Roche	Cat#5056489001
Terminator Exonuclease	Epicentre	Cat#TER51020
DNase I	Promega	Cat#M6101
Dynabeads Protein G	Invitrogen	Cat#10003D
rProtein A Sepharose Fast Flow	GE Healthcare	Cat#17-2179-02
Magna ChIP Protein G Magnetic beads	Millipore	Cat#16-662
EZview Red Anti-c-Myc Affinity Gel	Sigma-Aldrich	Cat#E6654
GFP Trap, coupled to agarose	ChromoTek	Cat#gta-20
Flg22 peptides	Sangon Biotech	N/A
AGO1N peptides	Sangon Biotech	N/A
Critical Commercial Assays		
pENTR/D-TOPO Cloning Kit	Invitrogen	Cat#450218
Gateway LR Clonase II Enzyme Mix	Invitrogen	Cat#11791-100
LA Taq DNA polymerase	Takara	Cat#RR900A

(Continued on next page)

Continued

REAGENT or RESOURCE	SOURCE	IDENTIFIER
M-MLV Reverse Transcriptase	Invitrogen	Cat#28025-013
SuperScript III Reverse Transcriptase	Invitrogen	Cat#18080085
SYBR Premix Ex Taq (Tli RNaseH Plus)	Takara	Cat#RR420A
RNeasy Plant Mini Kit (50)	QIAGEN	Cat#74904
ProteoSilver Silver Stain Kit	Sigma-Aldrich	Cat#PROT-SIL1
Agencourt AMPure XP beads	Beckman Coulter	Cat#A63881
NEXTflex ChIP-Seq Kit	Bioo Scientific	Cat#5143-02
NEXTflex RNA-Seq Kit	Bioo Scientific	Cat#5129-01
Deposited Data		
Raw and analyzed data	This paper	GEO: GSE95301
The Arabidopsis thaliana genome (TAIR10)	The Arabidopsis Information Resource	www.arabidopsis.org
Experimental Models: Organisms/Strains		
<i>Arabidopsis thaliana</i> : WT Col-0	N/A	N/A
<i>Arabidopsis thaliana</i> : WT Ler	N/A	N/A
<i>Arabidopsis thaliana</i> : <i>ago1-36</i>	Baumberger and Baulcombe, 2005	N/A
<i>Arabidopsis thaliana</i> : <i>ago1-25</i>	Morel et al., 2002	N/A
<i>Arabidopsis thaliana</i> : <i>hy1-2</i>	Kurihara et al., 2006	N/A
<i>Arabidopsis thaliana</i> : <i>dcl1-9</i>	Jacobsen et al., 1999	N/A
<i>Arabidopsis thaliana</i> : <i>dcl2-1 dcl3-1 dcl4-2</i>	Henderson et al., 2006	N/A
<i>Arabidopsis thaliana</i> : <i>dcl1-9 dcl2-1 dcl3-1 dcl4-2</i>	Ye et al., 2016	N/A
<i>Arabidopsis thaliana</i> : <i>swi3b-2</i>	Zhu et al., 2013	N/A
<i>Arabidopsis thaliana</i> : <i>swi3d-2</i>	Zhu et al., 2013	N/A
<i>Arabidopsis thaliana</i> : <i>syd-4</i>	Zhu et al., 2013	N/A
<i>Arabidopsis thaliana</i> : <i>brm-4</i>	Zhu et al., 2013	N/A
<i>Arabidopsis thaliana</i> : <i>coi1-1</i>	Yan et al., 2009	N/A
<i>Arabidopsis thaliana</i> : <i>pAGO1:GFP-AGO1 ago1-36</i>	This paper	N/A
<i>Arabidopsis thaliana</i> : <i>pAGO1:GFP-AGO1^{Y466AF467A} ago1-36</i>	This paper	N/A
<i>Arabidopsis thaliana</i> : <i>pAGO1:GFP-AGO1^{D848A} ago1-36</i>	This paper	N/A
<i>Arabidopsis thaliana</i> : <i>pSWI3B:SWI3B-myc</i>	This paper	N/A
<i>Arabidopsis thaliana</i> : <i>pSWI3B:SWI3B-myc ago1-36</i>	This paper	N/A
Oligonucleotides		
Primers for AGO1 ChIP-qPCR, see Table S6	This paper	N/A
Primers for Pol II ChIP-qPCR, see Table S6	This paper	N/A
Primers for quantitative RT-PCR, see Table S6	This paper	N/A
Primers for plasmid constructs, see Table S6	This paper	N/A
Recombinant DNA		
<i>pAGO1::GFP-AGO1</i>	Wang et al., 2011b	N/A
<i>pAGO1::GFP-AGO1^{Y466AF467A}</i>	This paper	N/A
<i>pAGO1::GFP-AGO1^{D848A}</i>	This paper	N/A
<i>p35S::SV40NLS-mCherry</i>	Ye et al., 2012	N/A
<i>p35S::SWI3B-GFP</i>	This paper	N/A
<i>p35S::SWI3D-GFP</i>	This paper	N/A
<i>p35S::BSH-GFP</i>	This paper	N/A
<i>p35S::myc-AGO1</i>	This paper	N/A

(Continued on next page)

Continued

REAGENT or RESOURCE	SOURCE	IDENTIFIER
p35S:3xflag-AGO1	Wang et al., 2011b	N/A
pSWI3B:SWI3B-myc	This paper	N/A
Software and Algorithms		
Image J 1.6.0	National Institutes of Health	https://imagej.nih.gov/ij/
Digimizer 3.1.1.	MedCalc Software	http://www.digimizer.com
Bowtie	Langmead et al., 2009	http://bowtie-bio.sourceforge.net/index.shtml
MACS2	Zhang et al., 2008	https://github.com/taoliu/MACS
TopHat	Trapnell et al., 2009	http://ccb.jhu.edu/software/tophat/index.shtml
Cuffdiff	Trapnell et al., 2012	http://cole-trapnell-lab.github.io/cufflinks/cuffdiff/
Samtools	Heinz et al., 2010	http://samtools.sourceforge.net/
Bedtools	Zhang et al., 2008	http://bedtools.readthedocs.io/en/latest/
HOMER	Trapnell et al., 2009	http://homer.ucsd.edu/homer/ngs/groseq/groseq.html
agriGO	Du et al., 2010	http://bioinfo.cau.edu.cn/agriGO/
ngs.plot	Shen et al., 2014	https://github.com/shenlab-sinai/ngsplot

CONTACT FOR REAGENT AND RESOURCE SHARING

Further information and requests for resources and reagents should be directed to and will be fulfilled by the Lead Contact, Yijun Qi (qiyijun@tsinghua.edu.cn).

EXPERIMENTAL MODEL AND SUBJECT DETAILS

Arabidopsis Columbia-0 (Col-0) ecotype and Landsberg erecta (Ler) ecotype were used in this study. *Arabidopsis* mutants ago1-36 (Baumberger and Baulcombe, 2005), ago1-25 (Morel et al., 2002), hyl1-2 (Kurihara et al., 2006), dcl1-9 (dcl1) (Jacobsen et al., 1999), dcl2-1 dcl3-1 dcl4-2 (dcl2/3/4) (Henderson et al., 2006), dcl1-9 dcl2-1 dcl3-1 dcl4-2 (dcl1/2/3/4) (Ye et al., 2016), swi3b-2, swi3d-2, syd-4, brm-4 (Zhu et al., 2013) and coi1-1 (Yan et al., 2009) have been described previously. Transgenic plants expressing pAGO1::GFP-AGO1, pAGO1::GFP-AGO1^{Y466AF467A}, pAGO1::GFP-AGO1^{D848A} and pSWI3B:SWI3B-myc in wild type and ago1-36 background were generated in this study.

Plants used for protoplasts isolation were grown in soil under a 10-h-light/14-h-dark photoperiod, otherwise plants were grown in soil or media under a 16-h-light/8-h-dark photoperiod at 22°C. For treatments with phytohormones or stresses, seeds were plated on 1/2 MS media containing 1% sucrose, stratified for 3 days at 4 °C in the dark, and then grown at 22°C. Ten-day-old seedlings were exposed to one of the following treatments: 50 µM of MeJA for 1 h, 10 µM of flg22 for 3 h, 40 µM of BTH for 24 h and 4°C (cold) for 6 h. For IAA treatment, 6-day-old seedlings were transferred to new 1/2 MS media and placed vertically for 4 days. Then they were grown on 1/2 MS containing 20 µM IAA for 1 h. MeJA (Sigma-Aldrich) was dissolved in ethanol to make a 200 mM stock solution. Flg22 (Sangon Biotech) was dissolved in water and prepared as a 100 mM stock solution. BTH (Sigma-Aldrich) was dissolved in water as a 40 µM working solution. IAA (Sigma-Aldrich) was dissolved in ethanol and prepared as 100 mM stock solution. Plants grown under the same condition were treated with the buffers and served as controls.

METHOD DETAILS**DNA Constructs and Plant Transformation**

pAGO1::GFP-AGO1 (Wang et al., 2011b) and p35S::SV40NLS-mCherry (Ye et al., 2012) have been described previously. For genetic complementation experiments, pEmycAGO1^{Y466AF467A} and pEmycAGO1^{D848A} were generated by site-directed mutagenesis using pEmycAGO1 (Mi et al., 2008) as the template and primers listed in Table S6. The AGO1^{Y466AF467A} and AGO1^{D848A} fragments were subsequently recombined into a modified destination vector pMDC43, in which the 35S promoter is replaced by the native AGO1 promoter (Wang et al., 2011b), resulting in pAGO1::GFP-AGO1^{Y466AF467A} and pAGO1::GFP-AGO1^{D848A}.

To test the interactions between AGO1 and subunits of the SWI/SNF complex in *Arabidopsis* protoplast, the full length cDNA fragments of SWI3B, SWI3D and BSH were amplified by RT-PCR using primers listed in Table S6, cloned into pENTR/D-TOPO (Invitrogen, 450218) and then transferred to the destination vector pEarleygate103 (Earley et al., 2006) through LR recombination, resulting in p35S::SWI3B, p35S::SWI3D and p35S::BSH-GFP. The AGO1 fragment in pEmycAGO1 was recombined into the

destination vector pMDC32 (Curtis and Grossniklaus, 2003) to create the construct *p35S::myc-AGO1*. *p35S::3xflag-AGO1* has been described (Wang et al., 2011b).

To generate the construct *pSWI3B::SWI3B-myc*, the genomic sequence of *SWI3B* including a 1.5-kb promoter was amplified from Col-0 genomic DNA using primers listed in Table S6, digested with *Bam*H1 and *Eco*RI, and then cloned into a modified pCAMBIA1305 vector with the 3xmyc coding sequence (Liu et al., 2014). All primers used for constructs are listed in Table S6.

Transgenic plants were generated by a floral dip method (Clough and Bent, 1998). *pAGO1::GFP-AGO1*, *pAGO1::GFP-AGO1^{Y466AF467A}*, *pAGO1::GFP-AGO1^{D848A}* and *pSWI3B::SWI3B-myc* were transformed into heterozygous *ago1-36* plants. Positive transformants were identified through selection for antibiotic resistance and confirmed by Western blot.

Protoplast Transfection

Protoplast preparation and PEG-mediated transfection were performed as described (Yoo et al., 2007). Briefly, the well expanded leaves from 4-week-old plants were cut into 0.5–1 mm leaf strips with fresh razor blades in 0.4 M mannitol solution. The leaf strips were submerged in enzyme solution (1.59% cellulase R10, 0.49% macerozyme R10, 0.4 M mannitol, 20 mM KCl, 20 mM MES, pH 5.7, 10 mM CaCl₂, 0.1% BSA), and then incubated in the dark for 3–4 h with gentle shaking (40–45 rpm). The protoplasts were filtered and washed with the same volume of pre-cold W5 solution (154 mM NaCl, 125 mM CaCl₂, 5 mM KCl and 2 mM MES, pH 5.7) for 3 times. After centrifugation at 100 g for 2 min, the protoplasts were suspended by pre-cold W5 solution and incubated on ice for 30 min. After centrifugation, the supernatants were discarded and the protoplasts were suspended by MMg solution (0.4 M mannitol, 15 mM MgCl₂, 4 mM MES, pH 5.7). For transfection, protoplasts (200 µl) were gently mixed with construct (20 µg) and 240 µl PEG/Ca solution (40% PEG4000, 100 mM CaCl₂, 0.2 M mannitol) for 20 min at room temperature. Then the transfected protoplasts were washed 3 times with W5 solution. Finally the transfected protoplasts were suspended with 1 mL W5 solution and cultured for 10–15 h under dim white light.

Confocal Fluorescence Microscopy

GFP and mCherry fluorescence in transfected protoplasts was observed 10 to 15 h after transfection using a Leica TCS SP5 inverted confocal microscope. The images were displayed as 3D projected stacks of 10–12 neighboring sections reconstructed by LAS AF Version 2.2.0.

Subcellular Fractionation

Subcellular fractionation was performed as described with minor modifications (Zhang et al., 2014). Three-week-old plants (about 1 g) were harvested, ground into fine powder in liquid nitrogen and suspended in Honda buffer (0.4M Sucrose, 2.5% Ficoll, 5% Dextran T40, 25 mM Tris-HCl, pH 7.4, 10 mM MgCl₂, 0.5% Triton X-100, 0.5 mM PMSF, 10 mM β-mercaptoethanol, RNase inhibitor and Roche protease inhibitor cocktail) (2 ml/g). The homogenate was filtered through double layers of Miracloth twice. The flow-through was centrifuged at 1,500 g for 5 min at 4 °C, and the supernatant was spun at 10,000 g for 10 min at 4 °C and collected as cytoplasmic fraction. The pellet was resuspended in 1 ml Honda buffer and centrifuged at 1,800 g for 5 min at 4 °C to pellet the nuclei. The pellet was then washed four times with Honda buffer and rinsed with PBS buffer (137 mM NaCl, 2.7 mM KCl, 10 mM Na₂HPO₄, 2 mM KH₂PO₄) containing 1 mM EDTA. Following that, the pellet was resuspended in 250 µl cold glycerol buffer (20 mM Tris-HCl, pH 7.9, 50% glycerol, 75 mM NaCl, 0.5 mM EDTA, 0.85 mM DTT, 0.125 mM PMSF and Roche protease inhibitor cocktail). The same volume of prechilled nuclei lysis buffer (10 mM HEPES, pH 7.6, 1 mM DTT, 7.5 mM MgCl₂, 0.2 mM EDTA, 0.3 M NaCl, 1M Urea, 1% NP-40, 0.5 mM PMSF, 10 mM β-mercaptoethanol, RNase inhibitor and Roche protease inhibitor cocktail) was then added and the mixture was vortexed, incubated for 2 min on ice, and centrifuged at 14,000 rpm for 2 min at 4 °C. The supernatant was collected as nucleoplasmic fraction and the resulting chromatin-associated pellet was rinsed with PBS buffer containing 1 mM EDTA before being resuspended in 250 µl cold glycerol buffer and 250 µl prechilled nuclei lysis buffer.

Chromatin Immunoprecipitation

ChIP assays were performed as previously described (Fang et al., 2015). Briefly, 10-day-old Col-0 and *ago1-36* seedlings (about 1.5 g), without or with hormone and stress treatments, were cross-linked in 1% formaldehyde for 20 min. Then the nuclei were isolated and resuspended in high salt nuclear lysis buffer (20 mM Tris-HCl, pH 7.5, 500 mM NaCl, 4 mM MgCl₂, 0.2% NP-40, 5 mM DTT, and Roche protease inhibitor cocktail). Chromatin was sonicated to an average size of 200–500 bp using the Bio-ruptor (Diagenode). After centrifugation at 16,000 g for 10 min, the supernatant was diluted 5-fold with dilution buffer (20 mM Tris-HCl, pH 7.5, 4 mM MgCl₂, 0.2% NP-40). AGO1 (Qi et al., 2005), myc (Abcam, ab32), Pol II (Abcam, ab817), Pol II Ser2P (Abcam, ab24758), or Pol II Ser5P antibody (Abcam, ab24759) was used to immunoprecipitate the protein-DNA complex. Rabbit IgG (Abmart, B30011) or mouse IgG (Abmart, B30010) was used as a negative antibody control for IP. After reverse cross-linking, digestion by proteinase K, the enriched DNA was purified for library construction for Illumina sequencing or for qPCR. The primers are listed in Table S6.

ChIP Sequencing Analysis

Libraries for ChIP-seq were generated using the NEXTflex ChIP-seq Kit (Bioo Scientific, 5143-02) according to the manufacturer's instructions. Briefly, Input and ChIP DNAs were end-repaired and ligated to adapters. Ligated products were amplified for 10–15 cycles using LA Taq DNA polymerase (Takara, RR900A), and the PCR products were cleaned by Agencourt AMPure XP beads (Beckman Coulter, A63881). Samples were barcoded and subjected to 50-bp single-end deep sequencing on the Illumina HiSeq2000 or

HiSeq2500 platform by Bionova Biotech (Beijing). For all ChIP-Seq datasets, reads were aligned to the *Arabidopsis* genome (TAIR10) using Bowtie ([Langmead et al., 2009](#)). Only unique alignments with up to 2 mismatches were retained and duplicate reads were removed by SAMtools ([Li et al., 2009](#)). Each mapped read was extended to 200 bp according to the average ChIP fragment length for further analysis. Peaks were identified by MACS2 ([Zhang et al., 2008](#)) with default parameters (q value $< 10^{-5}$). For AGO1 ChIP-seq, reproducible peaks (50% overlap) in two biological replicates of ChIP-seq in Col-0 were merged as primary AGO1 peaks. Reads pooled from two replicates were used to determine the ChIP signal on each peak. Genes that overlap (at least 50% for one side) with peaks in gene body, 1 kb upstream of the TSS, or 1 kb downstream of the TTS were considered to be peak associated genes.

For identification of differential AGO1 binding events in response to hormonal, biotic and abiotic stimuli, two sets of peaks from control or treated sample were pooled together and further merged if 50% of a peak region is covered by another. ChIP signals (IP-input, RPKM normalized) from peak regions in control or treated sample were calculated respectively. Peaks either only found under stimulus treatment condition or with fold enrichment (treatment/control) more than 2 were considered to be stimuli-induced AGO1 peaks.

Metaplots of AGO1 and Pol II ChIP-seq signals were made by calculating normalized sequencing reads within each 100 bp intervals around TSS and TTS of AGO1-bound genes. The distribution of AGO1 ChIP-seq reads across AGO1 peak regions in Col-0, *swi3b-2/+* and *brm-4* was made by ngs.plot program ([Shen et al., 2014](#)).

RNA Sequencing Analysis

Total RNA was purified from 10-day-old seedlings using RNeasy Plant Mini Kit (QIAGEN, 69104). Libraries for RNA-seq were generated using the NEXTflex RNA seq Kit (Bioo Scientific, 5129-01) according to the manufacturer's instructions. Briefly, RNAs were fragmented using NEXTflex RNA fragmentation buffer. Fragmented RNAs underwent first strand synthesis by superScript III reverse transcriptase (Invitrogen, 18080085) and second strand synthesis by second strand synthesis mix in the kit. Double stranded cDNAs were end-repaired and ligated to adapters. Ligated products were amplified for 12–15 cycles using LA Taq DNA polymerase (Takara, RR900A), and the PCR products were cleaned by Agencourt AMPure XP beads (Beckman Coulter, A63881). Samples were barcoded and subjected to Illumina sequencing by Bionova Biotech (Beijing). Sequencing reads were mapped to the *Arabidopsis* genome (TAIR10) using TopHat ([Trapnell et al., 2009](#)) and uniquely mapped reads with up to 2 mismatches were retained for further analysis. Cuffdiff ([Trapnell et al., 2012](#)) was used for calculating gene expression levels (normalized for FPKM, Fragments Per Kilobase of exon model per Million mapped reads) and differential gene expression analysis (q value < 0.05 , fold change > 1.5) with default settings.

Quantitative PCR

Quantitative PCR (qPCR) was performed using SYBR Premix EX Taq (TAKARA, RR420A) and DNA from ChIP or cDNA. For analysis of mature mRNA, cDNA was generated using M-MLV reverse transcriptase (Invitrogen, 28025-013) and oligo (dT). For analysis of transcripts from exonic and intronic regions, cDNA was generated using SuperScript III reverse transcriptase (Invitrogen, 18080085) and random hexamer primers (Invitrogen, N8080127). The level of *Actin* mRNA was detected in parallel and used for normalization. Primer sequences are provided in the [Table S6](#).

Nuclear Run-On

Nuclear Run-On assay was performed as described ([Roberts et al., 2015](#)) except that nuclei were isolated from 10-day-old seedlings as described ([Wang et al., 2011b](#)). Approximately 1 million nuclei were resuspended in nuclei storage buffer (50 mM Tris-HCl, pH 7.8, 5 mM MgCl₂, 20% glycerol, 1 mM DTT, 0.44 M sucrose) and then mixed with an equal volume of reaction buffer (50 mM Tris-HCl, pH 7.5, 5 mM MgCl₂, 1 mM DTT, 150 mM KCl, 0.2% sarkosyl, 40 units RNase inhibitor, 1 mM ATP, 1 mM GTP, 1 mM CTP and 1 mM Br-UTP). After incubation at 30 °C for 10 min, the reaction was stopped by addition of Trizol reagent (Invitrogen). RNAs were extracted and treated with DNase I (Promega) to remove genomic DNA. The purified RNAs were incubated with 2 µg anti-BrdU antibody (abcam, ab1893) at 4 °C for 2 h and then subjected to immunoprecipitation with Dynabeads Protein G (Invitrogen, 10003D) pre-coated with yeast tRNA (Invitrogen, AM7119) for 1 h. Precipitated RNAs were extracted by Trizol reagent and used for cDNA synthesis and qPCR analysis. Primers used for qPCR are listed in [Table S6](#).

Global Run-On Sequencing Analysis

GRO-seq was performed as described ([Wang et al., 2011a](#)). Briefly, ~5X10⁶ nuclei were run on for 5 min at 30 °C. The reactions were stopped by addition of Trizol and RNAs were extracted. After digestion with Terminator exonuclease (Epicentre, TER51020) and fragmentation, nascent RNAs were enriched twice for 5-bromo-UTP (BrUTP) by immunoprecipitation. After end repair and decapping, libraries were constructed and sequenced on the Illumina Hiseq 2500 platform under single-end, 50-bp conditions. Sequencing reads were mapped to the *Arabidopsis* genome (TAIR10) with Bowtie ([Langmead et al., 2009](#)) and Metaplots were generated by the HOMER software ([Heinz et al., 2010](#)) with default settings.

Identification of Small RNAs and Proteins Associated with Nuclear AGO1

Nuclei were isolated from 10-day-old seedlings as described ([Wang et al., 2011b](#)). The purified nuclear pellets were homogenized with nuclear lysis buffer (20 mM Tris-HCl, pH 8.0, 500 mM KCl, 0.5% Triton X-100, 25% glycerol, 1.5 mM MgCl₂, 0.5 mM EDTA, 5 mM DTT, protease inhibitor cocktail and 1 mM PMSF) and incubated for 20 min at 4 °C. After centrifugation at 15,000 g for 10 min at 4 °C, the supernatant was collected as nuclear extracts. The nuclear extracts were diluted with 2.3 volume of dilution buffer

(20 mM Tris-HCl, pH 8.0, 0.5% Triton X-100, 1.5 mM MgCl₂, 0.5 mM EDTA, 5 mM DTT, protease inhibitor cocktail and 1 mM PMSF). After pre-clearing by protein A agarose beads, the nuclear extracts were incubated with AGO1 antibody or IgG for 2 h. Then protein A agarose beads were added and incubated for another 2 h. The beads were washed with wash buffer (20 mM Tris-HCl, pH 8.0, 150 mM KCl, 0.5% Triton X-100, 25% glycerol, 1.5 mM MgCl₂, 0.5 mM EDTA) 4 times, each time 5 min. The AGO1 complexes were then eluted with AGO1N peptide solution (0.5 mg/mL) at 16°C for 30 min. A small fraction of the immunoprecipitates was separated by SDS-PAGE and silver stained for quality control.

To characterize nuclear AGO1-associated sRNAs, sRNAs were extracted from the immunoprecipitates and resolved on a 15% denaturing PAGE gel. RNAs of 18–30 nt were gel-purified and subjected to library construction as described (Mi et al., 2008). Briefly, purified sRNAs were ligated with 3' adaptors and then 5' adaptors. Reverse transcriptions were performed using the ligated sRNAs as templates. Then cDNAs were amplified by PCR. Libraries were sequenced on the Illumina HiSeq 2000 platform by Bionova Biotech (Beijing) under single-end, 50-bp conditions. After removal of adapters and low-quality reads, sRNA-seq reads were mapped to the *Arabidopsis* genome (TAIR10 version) with Bowtie (Langmead et al., 2009). Only perfectly matched sRNAs, excluding those mapped to known classes of RNAs such as rRNAs, tRNAs, snRNAs, snoRNAs, miRNAs and tasiRNAs, were kept for further analysis.

To identify proteins associated with nuclear AGO1, the IgG and AGO1 immunoprecipitates were run on a 12% SDS-PAGE gel, followed by silver staining with the ProteoSilver Silver Stain Kit (Sigma, PROT-SIL1). Whole proteins were purified from the gel and subjected to mass spectrometric analysis on the LTQ mass spectrometer equipped with a nano-ESI ion source. Data were searched using Mascot server against the International Protein Index (IPI) Database.

Gene Ontology Analysis

Gene Ontology enrichment analysis was performed by agriGO (Du et al., 2010). Lists of AGO1-bound genes under normal conditions and various stimuli were compared with the pre-calculated background using the Singular Enrichment Analysis (SEA) method. Fisher's exact tests with Yekutieli adjustment were used for the calculation of *p*-values and false discovery rates (FDRs). Terms with FDR<0.05 were considered to be enriched.

Generation of the Control Gene Sets

To generate control gene sets with similar expression levels as AGO1-bound genes used in Figures 2B, 3A, 3C, S2E, and S2G, 894 AGO1-bound genes were first sorted into ten groups by highest to lowest expression levels. Non-AGO1-bound genes were then sorted into ten groups based on the ranges of gene expression levels defined by the ten groups of AGO1-bound genes. 894 genes were randomly selected from the groups of non-AGO1-bound genes by using RANDOM function in Shell for 51 times and ranked by highest to lowest expression. The expression levels of 51 sets of selected genes were put into one table (one column stands for one set of genes) and the gene with median expression value of each row was used to constitute the control group of genes.

To generate control gene sets with similar expression levels as AGO1-bound genes used in Figure 4A, AGO1-bound genes and non-AGO1-bound genes were sorted into ten groups as described above. 894 genes were randomly selected from groups of non-AGO1-bound genes by using RANDOM function in Shell for 1,000 times. sRNA signal (RPKM) for each gene was calculated. The sRNA signals of 1,000 sets of selected genes were put into one table (one column stands for sRNA signals for one set of genes) and the mean value of sRNA signals for each gene set was used to generate the scatter plot.

Co-immunoprecipitation

Immunoprecipitation of tagged proteins from transfected *Arabidopsis* protoplasts was carried out as described (Wang et al., 2011b). In brief, total proteins were extracted from the transfected protoplasts by extraction buffer (20 mM Tris-HCl, pH 7.5, 100 mM NaCl, 4 mM MgCl₂, 0.2% NP-40, 5 mM DTT, and Roche protease inhibitor cocktail). After centrifugation, the supernatants were incubated with anti-c-Myc Affinity Gel (Sigma-Aldrich, E6654) or GFP-binding protein (GBP)-conjugated beads for 2 h. The beads were washed with wash buffer (20 mM Tris-HCl, pH 7.5, 100 mM NaCl, 4 mM MgCl₂, 0.2% NP-40) 4 times, each time 5 min. Then The Myc- bound or GBP-bound protein complexes were boiled in SDS loading buffer. The immunoprecipitates were analyzed by Western blot.

Western Blot Analysis

Total protein extracts or immunoprecipitates were separated by SDS-PAGE, transferred to PVDF membranes, and detected by specific antibodies against AGO1 (Qi et al., 2005), tubulin (Sigma-Aldrich, T5168), histone H3 (Sigma-Aldrich, H0164), PEPC (Abcam, ab34793), Pol II (Abcam, ab817), Pol II Ser2P (Abcam, ab24758), or Pol II Ser5P (Abcam, ab24759), flag (Sigma-Aldrich, F1804), GFP (Roche, 11814460001) or myc (Roche, 11667203001).

Root Measurement

For measuring MeJA-mediated root growth inhibition, seeds were plated on 1/2 MS media supplemented with 0, 5, 20 or 40 µM of MeJA, stratified for 3 days at 4 °C in the dark and then grown at 22 °C under 16-h light/ 8-h dark photoperiod for 10 days. For each treatment, more than 20 seedlings were photographed and root length was measured with Digimizer 3.1.1.0 (<http://www.digimizer.com>).

QUANTIFICATION AND STATISTICAL ANALYSIS

Quantification of protein levels was performed by measuring the intensities of the bands from Western blot using ImageJ. All quantitative PCR data are presented as the mean of three biological replicates \pm standard deviation (SD). Two-tailed Student's t tests were used to determine the difference between two groups. The cutoff for significance was 0.05. All box plots, scatter plots, metaplots in this study were made by using R programs (www.R-project.org/) (R Core Team, 2014).

In Figures 1C, 1D, and S6, two-tailed Fisher's exact tests were used to calculate *p*-values for analysis of the significant enrichment levels of examined features in AGO1-bound regions compared to the genome. The cutoff for significance was 0.05.

In Figures 2A and 2B, Mann-Whitney-Wilcoxon tests were used to calculate *p*-values for analysis of the levels of significant difference between the distributions of two populations. The cutoff for significance was 0.05.

For Gene Ontology enrichment analysis in Figure 6 and Table S4, Fisher's exact tests with Yekutieli adjustment were used for the calculation of *p*-values and false discovery rates (FDRs). Terms with FDR<0.05 were considered to be enriched.

DATA AND SOFTWARE AVAILABILITY

All ChIP-seq, RNA-seq, GRO-seq, and small RNA-seq data have been deposited in GEO under the series reference GEO: GSE95301.